Robust Space Trajectory Design using Belief Stochastic Optimal Control

Cristian Greco*
University of Strathclyde, Glasgow, G1 1XJ, UK

Stefano Campagnola†
Jet Propulsion Laboratory, California Institute of Technology, Pasadena, CA 91109, USA

Massimiliano Vasile‡
University of Strathclyde, Glasgow, G1 1XJ, UK

This paper presents a belief-based formulation and a novel approach for the robust solution of optimal control problems under uncertainty. The introduced formulation, based on the Belief Markov Decision Process model, reformulates the control problem directly in terms of uncertainty distributions, called beliefs, rather than on realisations of the system state. Successively, an approach inspired by navigation analysis is developed to transcribe and solve such problem in the presence of observation windows, employing a polynomial expansion for the dynamical propagation. Finally, the developed method is applied to the robust optimisation of a flyby trajectory of Europa Clipper mission in a scenario characterised by knowledge, execution and observation errors.

I. Introduction and Motivation

Space trajectories are typically optimised to meet the science and flight system constraints in a nominal scenario. However, in real-life applications, perfect compliance to the reference trajectory is impossible to achieve as uncertainty always affects the system; uncertainty can be due to imperfect state knowledge, imperfectly known dynamical parameters, missed thrust events or execution errors.

In the design phase, the reference trajectory robustness and reliability to these uncertainties is usually evaluated a posteriori through a navigation analysis and the nominal design adjusted through several iterations. The robustness and reliability evaluation is carried out by assessing the mission outcome when the trajectory is affected by different uncertainty realizations. To improve the robustness, small tweaks to the trajectory are ensured either by adding propellant margin and enforced coasting arcs for trajectory correction maneuvers (TCM), or by reducing the thrust level. Hence, this iterative procedure mainly treats the nominal trajectory optimisation as decoupled from the uncertainty treatment phase. This process is generally time-consuming and may lead to sub-optimal trajectories with over-conservative margins.

Recent development in components and launchers are now enabling deep-space microsat and nanosat missions. Such spacecraft have limited orbit control capabilities (limited DV), large uncertainties in the state knowledge (limited ground station access) and in the execution (low TRL components), and low possibility of margins and system redundancy (limited size and cost). Therefore, for these missions, the design of the trajectory is driven by its robustness to uncertainties even more critically. While trajectory optimisation under uncertainty is an enabling methodology for small spacecraft, large traditional missions would also benefit from stochastic trajectory optimisation both in terms of performance improvement, because the stochastic optimal trajectory generally differs from the deterministic one with empirical margins, and in terms of a reduction in the number of design iterations.

As said, currently the main practical approach is to allocate a posteriori empirical margins [1, 2]. Recent works generated robust trajectories employing different formulations of the stochastic optimal control problem. Model predictive control or stochastic closed-loop formulations were used to account for correction terms in the control profile [3, 4]. The case of a temporary engine failure were investigated by stochastic programming [5, 6]. Differential

*PhD Candidate, Aerospace Centre of Excellence, University of Strathclyde, *c.greco@strath.ac.uk*; Member AIAA.
†Mission Design Engineer, Outer Planet Mission Analysis Group, *stefano.campagnola@jpl.nasa.gov*; Member AIAA.
‡Professor, Aerospace Centre of Excellence, University of Strathclyde, *massimiliano.vasile@strath.ac.uk*; Member AIAA.

dynamic programming was applied to trajectory optimisation with an expected value formulation for Gaussian-modelled uncertainties [7]. Approaches based on evidence theory to model uncertainty was developed for the robust optimisation of transfers under system and dynamical uncertainties [8–10].

As a contribution to this recent field and to the maturity of stochastic approaches, this paper presents novel developments in stochastic optimal control problems for the robust design of space trajectories which extend previous research on optimal control under epistemic uncertainty [11]. This previous work introduced a general formulation and a novel generalised multiple shooting stochastic transcription for trajectory optimisation under uncertainty, capable of handling a wide range of uncertainty models (parametric, non-parametric, imprecise set of distributions, etc.), while keeping the familiar notation of deterministic optimal control problems. The present work generalises such method to incorporate navigation in the formulation, thus including orbit determination (OD) arcs and closed-loop controllers, to update the knowledge of the spacecraft state uncertainty in the presence of observations. This approach enables the direct coupling of trajectory optimisation with navigation analysis by incorporating an uncertainty quantification (UQ) procedure within the optimisation cycle. To this end, this paper also introduces a new efficient UQ approach for nonlinear navigation analysis (NA) based on generalised polynomial expansions, which generalises the linear NA [12, 13] to higher order representations of the dynamics.

The final goal is the generation of optimal nominal trajectories which are most robust and reliable to the possible uncertainty realisations, that is optimally minimising a statistical objective index while respecting stochastic constraints. Moreover, this method improves the overall trajectory design process by helping reducing the number of design iterations.

More in detail, first a formulation based on the Belief Markov Decision Process (BMDP) [14] is introduced to directly model the problem in terms of uncertainty distributions. This is particularly suited to model the inference step necessary for the state knowledge update when an orbit determination campaign is carried out. While BMDP is typically used to find optimal closed-loop controls in problems with a discrete state space, the formulation presented here is general enough to address both optimal open- and closed-loop control laws in continuous state space applications with sparse observation feedback. The optimised solution resulting from this approach is highly informative as it determines both the nominal control profile and a general control policy for possible deviations due to uncertainty, hence directly providing empirical margins for correction manoeuvres. Furthermore, BMDP is defined for precise probability distributions only, whereas the formulation employed here can accommodate *epistemic* and *imprecise* uncertainties as well. In addition, such formulation is generalised to encompass the class of problems involving sensor control, i.e. when the measurement policy itself has to be optimised, e.g. optimal planning of orbit determination arcs [15, 16], scheduling of trajectory correction maneuvers [17], science orbit design with coupled optimisation of the trajectory and measurements, and so on.

Successively, a practical approach to the solution of the optimal control problem under uncertainty (OCPUU) is proposed. By taking inspiration from navigation analysis, possible observation realisations are drawn with a Monte Carlo technique, and the uncertainty updates of orbit determination are solved with a sequential filter exploiting the developed polynomial NA.

Finally, the developed method is applied to the robust optimisation of a leg of Europa Clipper flyby tour [18], a scenario where proper uncertainty treatment is crucial to ensure appropriate close-approach conditions and low probability of impact. The OCPUU formulation is employed to optimise the trajectory statistical ΔV, while respecting *expected value* and *chance* constraints. The modelled uncertainty stems from knowledge error in the initial spacecraft state, from execution errors introduced by the thrust pointing and magnitude inaccuracies when operating the engine, and by measurement and sensor noises.

The remainder of the paper is structured as follows. Section II presents the overall uncertain scenario and the development of the belief stochastic optimal control formulation, which can be used to frame a large variety of problems in space trajectory design. Section III then introduces the stochastic transcription needed to convert the stochastic optimal control problem into a discrete one which can be numerically solved. Specifically, this sections addresses in depth how to incorporate measurement information in the robust trajectory design process, presents the polynomial NA approach employed, and discusses practical strategies to propagate and update the uncertainty in different cases. In Section IV, the developed methodology is applied to the robust optimisation of one part of the Europa Clipper flyby tour. Here, the problem is first modelled and framed under the developed OCPUU formulation, and then the developed optimisation approach is applied to solve for the robust trajectory. Finally, Section V concludes the paper with the final remarks and a discussion on possible future applications.

II. Stochastic Optimal Control Formulation

The deterministic optimal control problem can be formulated as

$$\min_{\mathbf{u},\,\mathbf{p}^x} \; J = \Phi(t_f, \mathbf{x}_f) + \int_{t_0}^{t_f} L(t, \mathbf{x}, \mathbf{u}, \mathbf{p}^x)\, dt \tag{1a}$$

$$\text{s.t.} \quad \dot{\mathbf{x}} = f(t, \mathbf{x}, \mathbf{d}, \mathbf{u}, \mathbf{p}^x) \tag{1b}$$

$$\mathbf{g}(t, \mathbf{x}, \mathbf{d}, \mathbf{u}, \mathbf{p}^x) \in \boldsymbol{G} \tag{1c}$$

$$\boldsymbol{\psi}(t_0, \mathbf{x}_0, t_f, \mathbf{x}_f) \in \boldsymbol{\Psi}\ , \tag{1d}$$

where t is the independent variable, $\mathbf{x}$ the state variable, $\mathbf{d}$ are static model parameters, $\mathbf{u}$ is the control law, while $\mathbf{p}^x$ are static control parameters, e.g. maneuvers times. Such deterministic optimal control problem aims at finding the optimal control profile $\mathbf{u}^*$ and static control parameters $\mathbf{p}^{x*}$ which minimise the objective function in Equation (1a) while respecting the dynamical nonlinear equations of motion in Equation (1b), path constraints in Equation (1c), and boundary conditions in Equation (1d). Often, a discretised version of the optimal control problem is employed where the trajectory is divided in arcs and the differential equations replaced by their integral counterparts. Indeed, control problems are typically implemented digitally and the discretised solution converges to the time-continuous one for decreasing discretisation arc width.

When uncertainty is taken into account, such formulation cannot be employed anymore. Hence, this section introduces the stochastic formulation of optimal control problems that serves as framework to find trajectories which are both optimal and robust to uncertainties.

A. Aleatoric Uncertainty

The stochastic optimal control problem addressed in this paper is defined by the following uncertain elements and probability distributions:

- *sources of uncertainty*: $\mathbf{X}_0$, $\mathbf{D}$

  uncertain knowledge of the initial conditions, now modelled as a random variable with distribution $\mathbf{X}_0 \sim P_{\mathbf{X}_0}$, and of the model parameters, likewise modelled as random variables $\mathbf{D} \sim P_{\mathbf{D}}$. Execution errors can be modelled within $\mathbf{D}$, while the control law $\mathbf{u}$ is deterministic. The uncertain variables $\mathbf{D}$ are nuisance parameters to be taken into account but not to be estimated. We will consider the case of uncertain parameters partitioned as

  $$\mathbf{D} = \left[\mathbf{D}_0, \mathbf{D}_1, \ldots, \mathbf{D}_{N-1}\right],$$

  that is $\mathbf{D}_k$ affects the dynamical equations only in the discretised time interval $t \in [t_k, t_{k+1})$. Uncertain model parameters which impacts the dynamical model in different (or all) time sub-intervals should be repeated in each corresponding $\mathbf{D}_k$.

- *dynamical evolution*: $\mathbf{X}_k = F^k_{k-1}(\mathbf{X}_{k-1}, \mathbf{D}_{k-1}, \mathbf{u}_{k-1}, \mathbf{p}^x_{k-1})$

  $\mathbf{X}_0$ and $\mathbf{D}$, together with Equation (1b), induce the state at a later time to be a random variable $\mathbf{X}_t$ through the push-forward measure resulting from the pointwise map

  $$\mathbf{x}_k = F^k_{k-1}(\mathbf{x}_{k-1}, \mathbf{d}_{k-1}, \mathbf{u}_{k-1}, \mathbf{p}^x_{k-1}) = \mathbf{x}_{k-1} + \int_{t_{k-1}}^{t_k} f(\tau, \mathbf{x}, \mathbf{d}_{k-1}, \mathbf{u}_{k-1}, \mathbf{p}^x_{k-1})\ d\tau\ , \tag{2}$$

  which is the integral form of the dynamical system equations. Hence, let $P\left(\mathbf{X}_k \middle| \mathbf{X}_{k-1}, \mathbf{u}_{k-1}, \mathbf{p}^x_{k-1}\right)$ be the state transition probability density describing the probabilistic dynamical evolution of the system due to uncertainty in $\mathbf{D}_{k-1}$. A discretised formulation is now employed, therefore the control profile $\mathbf{u}_k$ and optimisable static parameters $\mathbf{p}_k$ are defined for each k-th time interval $[t_k, t_{k+1})$.

- *observation step*: $\mathbf{Y}_k = h_k\left(\mathbf{X}_k, \mathcal{E}_k, \mathbf{p}^y_{k-1}\right)$

  observations are employed to reduce the uncertainty associated to the system state. The received observation $\mathbf{y}_k$ is a realisation of a random variable $\mathbf{Y}_k$ which depends on the uncertain state $\mathbf{X}_k$, sensor and environment noises modelled by the random variable $\mathcal{E}_k$ at time t_k, and the sensor action $\mathbf{p}^y_{k-1}$ which can be optimised, e.g. time or

type of observation. The sensor action influences how the belief state updates as it directly impacts the observation value. For ease of notation, the sensor action at time t_{k-1} controls the observation $\mathbf{y}_k$ at time t_k. Hence, let $P\big(\mathbf{Y}_k \,|\, \mathbf{X}_k,\, \mathbf{p}^y_{k-1}\big)$ be the conditional observation probability density describing the observation likelihood. This relations expresses that, given $\mathbf{X}_k$ and the sensor action $\mathbf{p}^y_{k-1}$, the density function of $\mathbf{Y}_k$ is completely determined by $\mathcal{E}_k$ [19].

Given these definitions, the stochastic optimal control problem under consideration is well described as a Partially Observable Markov Decision Process [20], i.e. when the state is observed only through indirect measurements. This model can be re-framed as a Belief Markov Decision Process [14], which employs an advantageous belief state representation. That is, the state of the model is not a specific realisation $\mathbf{x}_k$, but rather the state is the probability distribution $P_{\mathbf{X}_k}$ of $\mathbf{X}_k$. The probability distribution of the dynamical system state is henceforth called *belief* state. The main advantage of such formulation is that the belief state is now completely observable as at any time the probability distribution is known, whereas the specific state realisation is not.

Let $\mathbf{p} = [\mathbf{p}^x,\, \mathbf{p}^y]$ be the vector of optimisable static parameters, respectively containing both the control and sensor actions to be optimised. Hence, the optimal control problem under uncertainty (OCPUU) is formulated as

$$\min_{\mathbf{u},\,\mathbf{p}} \; J = \sum_{k=0}^{N-1} C\big(\mathbf{X}_k, \mathbf{u}_k, \mathbf{p}_k\big) + C_N\big(\mathbf{X}_N\big) \tag{3a}$$

$$\text{s.t.} \;\; \mathbf{X}_k = \mathcal{T}\big(\mathbf{X}_{k-1},\, \mathbf{D}_{k-1},\, \mathcal{E}_k,\, \mathbf{u}_{k-1}, \mathbf{p}_{k-1}\big) \tag{3b}$$

$$G\big(\mathbf{X}_k, \mathbf{u}_k, \mathbf{p}_k\big) \in \mathbf{\Phi}_{\mathbf{G}} \qquad \text{for } k = 0, \ldots, N-1 \tag{3c}$$

$$G_N\big(\mathbf{X}_N\big) \qquad \in \mathbf{\Phi}_{\mathbf{G}_N} \tag{3d}$$

$$\mathbf{X}_0 \sim P_{\mathbf{X}_0} \qquad\qquad , \tag{3e}$$

where the time discretisation in sub-intervals $[t_k, t_{k+1})$ is employed. Equation (3a) is the objective index defined as sum of real-valued cost functions C and C_N, respectively for intermediate and final times, which take as input the state, as random variable, and the controls, and return a deterministic value, e.g. its expected value or the probability of an event. Similarly, G and G_N are real-valued constraint functions expressed with a set inclusion condition, i.e. feasible in $\mathbf{\Phi}_{(\cdot)}$, to represent simultaneously equality and inequality constraints. Equation (3e) expresses the initial condition for the belief state $\mathbf{X}_0$. Finally, the dynamical equations describing the pointwise motion in Equation (1b) have been substituted by the transition function $\mathcal{T}$ in Equation (3b), which describes how the belief state evolves in time and after an observation update. In direct approaches, the continuous control profile is parameterised with a suitable functional relationship, and its parameters optimised by a numerical solver to find an optimal policy.

This belief formulation is very general and therefore it is suitable to frame a large range of problems in trajectory optimisation. Indeed, depending on the practical problem to be solved and on design choices, the generality of C and G functions allows the mission designer to impose objective and constraints in diverse fashions, e.g. in *expected value*, in *probability* (chance constraints), and so on, depending on the specific case to solve. Furthermore, since no assumptions are made on the nature of the probability distributions describing the uncertainties, or on the transition function to propagate them, this formulation is appropriate also to model the uncertainty structure of realistic and complex applications. This formulation further enables the concurrent optimisation of the *open-loop* thrust profile, the *closed-loop* controllers and orbit determination parameters, thus coupling the trajectory optimisation process with the navigation analysis.

In general, Problem (3) has no closed form solution, just like the deterministic optimal control problem. Hence, a practical approach is needed to convert the dynamical control problem into a static constrained one, which is possible to solve with well-established numerical routines, e.g. NLP solvers. The next section will present the development of a stochastic transcription enclosing observation steps for the practical solution of the stochastic optimal control problem.

B. Epistemic Uncertainty

In some uncertain scenarios, the density function of a random variable is partially unknown, and a precise specification is not possible. This is often the case with interval-valued model parameters, e.g. asteroid physical characteristics, or poorly characterised systems, e.g. sensor noises, low TRL thrusters, and so on.

In such cases, a stochastic variable is modelled as epistemic uncertainty, that is when its density function is specified

within a set rather than uniquely defined. Therefore, the distribution of the generic random variable $\mathbf{Z}$ is set-valued as

$$\mathbf{Z} \sim P(\mathbf{Z}) \in \mathcal{P}_{\mathbf{Z}} \,. \tag{4}$$

For the considered applications, $\mathbf{Z}$ can represent the initial conditions, model parameters or sensor noise equivalently. The imprecise set of distributions can be specified in different ways. One alternative is to parameterise the set with epistemic parameters λ as

$$P_{\mathbf{Z}} \in \mathcal{P}_{\mathbf{Z}} = \left\{ P_{\mathbf{Z}}(\mathbf{z};\lambda) \,|\, \lambda \in [\lambda_l, \lambda_u] \right\} , \tag{5}$$

where λ_l and λ_u are respectively the lower and upper parameter values. This option is to be chosen when the underlying stochastic distribution is known, but some of its parameters are not completely characterised, e.g. a set of Gaussians with interval-valued mean or covariance. Another alternative is to specify lower and upper functions, and allowing each distribution between them to be a feasible one as

$$P_{\mathbf{Z}} \in \mathcal{P}_{\mathbf{Z}} = \left\{ P_{\mathbf{Z}}(\mathbf{z}) \,|\, P^L_{\mathbf{Z}}(\mathbf{z}) \leq P_{\mathbf{Z}}(\mathbf{z}) \leq P^U_{\mathbf{Z}}(\mathbf{z}) \;\; \forall \mathbf{z} \in \Omega_{\mathbf{z}} \right\} , \tag{6}$$

where $P^L_{\mathbf{Z}}$ and $P^U_{\mathbf{Z}}$ are the lower and upper distributions. The latter case is known as imprecision and models the uncertain scenarios when the family of distributions is unknown.

Epistemic uncertainty on either of these stochastic variables causes the belief state to be set-valued itself as

$$\mathbf{X}_k \sim P_{\mathbf{X}_k} \in \mathcal{P}_{\mathbf{X}_k} \,. \tag{7}$$

Being the constraints and objective function maps from the probability function space to the real space, under epistemic uncertainty their output is interval-valued as

$$G(\mathbf{X}_k) \in [\, \underline{G}, \overline{G} \,] \;\text{ for }\; P_{\mathbf{X}_k} \in \mathcal{P}_{\mathbf{X}_k} \,, \tag{8}$$

where the lower and upper bounds are defined as

$$\begin{aligned} \underline{G}(\mathbf{X}_k) &= \inf_{P_{\mathbf{X}_k} \in \mathcal{P}_{\mathbf{X}_k}} G(\mathbf{X}_k) \\ \overline{G}(\mathbf{X}_k) &= \sup_{P_{\mathbf{X}_k} \in \mathcal{P}_{\mathbf{X}_k}} G(\mathbf{X}_k) \,, \end{aligned} \tag{9}$$

with the same notation holding for the objective functions C.

Therefore, for the epistemic setting the OCPUU as formulated in Equation (3) becomes

$$\min_{\boldsymbol{\mu} \in \mathcal{U}} \; J = \sum_{k=0}^{N-1} \overline{C}(\mathbf{X}_k, \mathbf{u}_k) + \overline{C}_N(\mathbf{X}_N) \tag{10a}$$

$$\text{s.t.} \;\; \mathbf{X}_k = \mathcal{T}\left(\mathbf{X}_{k-1}, \mathbf{D}_{k-1}, \mathcal{E}_k, \mathbf{u}_{k-1}\right) \tag{10b}$$

$$\underline{G}(\mathbf{X}_k, \mathbf{u}_k) \in \boldsymbol{\Phi}_{\underline{\mathbf{G}}} \,, \;\; \overline{G}(\mathbf{X}_k, \mathbf{u}_k) \in \boldsymbol{\Phi}_{\overline{\mathbf{G}}} \quad \text{for } k = 0, \ldots, N-1 \tag{10c}$$

$$\underline{G}_N(\mathbf{X}_N) \;\in \boldsymbol{\Phi}_{\underline{\mathbf{G}}_N}, \; \overline{G}_N(\mathbf{X}_k) \;\in \boldsymbol{\Phi}_{\overline{\mathbf{G}}_N} \tag{10d}$$

$$\mathbf{X}_0 \sim P_{\mathbf{X}_0} \in \mathcal{P}_{\mathbf{X}_0} \qquad . \tag{10e}$$

For the objective index, the epistemic worst-case scenario $\overline{C}$ is selected for this formulation to obtain a conservative robust solution, although different choices are possible. For the constraints, their lower and upper bounds can be independently constrained depending on the specific application. This setting includes the case when the whole interval $[\, \underline{G}, \overline{G} \,]$ should be contained in one compact set, in which case $\boldsymbol{\Phi}_{\underline{\mathbf{G}}} = \boldsymbol{\Phi}_{\overline{\mathbf{G}}}$.

III. Shooting Transcription

Solving an optimal control problem under uncertainty requires propagating the belief state from the initial condition in Equation (3e) through the dynamics, and update it at observation times with the received observations. This task can be tackled in a number of ways, e.g. Monte Carlo, just like the deterministic optimal control problem can be solved with different transcriptions. Although Monte Carlo methods for uncertainty propagation are straightforward to employ

as each sample can be propagated through the deterministic point-wise maps, they are often too expansive to be used within an optimisation cycle due to their slow convergence.

This section presents a shooting-like stochastic transcription for the optimal control problem in Problem (3), which employs a direct propagation of the uncertainty distribution. Specifically, it generalises the shooting transcription developed in [11] to the presence of orbit determination arcs and controllers.

In the general nonlinear case, the distribution of the belief state $\mathbf{X}_{k+1}$ is computed with a two-step approach typical of sequential state estimation filtering algorithms [21]:

- $\mathcal{T}_{predict}$: the belief state is propagated from t_k to t_{k+1} with the *Chapman-Kolgomorov* equation employing the conditional transition probability as

$$P^{-}_{\mathbf{X}_k} = p(\,\mathbf{x}_k \,|\, \mathbf{y}_{1:k-1}, \mathbf{u}_{0:k-1}, \mathbf{p}_{0:k-1}) = \int p(\mathbf{x}_k|\,\mathbf{x}_{k-1}, \mathbf{u}_{k-1}, \mathbf{p}^x_{k-1})\; p(\mathbf{x}_{k-1}|\,\mathbf{y}_{1:k-1}, \mathbf{u}_{0:k-1}, \mathbf{p}_{0:k-1})\, d\mathbf{x}_{k-1}\;, \tag{11}$$

  where the superscript $(\cdot)^-$ indicates that the distribution results from a dynamical prediction, $\mathbf{y}_{1:k}$ are all the observations up to time t_k, and $\mathbf{u}_{0:k-1}$ and $\mathbf{p}_{0:k-1}$ are all the control profile and parameters until time t_{k-1}. The control histories $\mathbf{u}_{0:k-2}$ and $\mathbf{p}_{0:k-2}$ disappear in the transition probability because the belief state $\mathbf{X}_k$ is conditionally independent on it given the belief state at the previous time $\mathbf{X}_{k-1}$ (Markov property). Essentially, Equation (11) is the belief counterpart of the point-wise dynamical propagation F^k_{k-1} in Equation (2), therefore it is used to propagate the state distribution itself rather than the state realisations.

- $\mathcal{T}_{update}$: the belief state is updated using the Bayes' inference rule as

$$P_{\mathbf{X}_k} = p(\mathbf{x}_k \,|\, \mathbf{y}_{1:k}, \mathbf{u}_{0:k-1}, \mathbf{p}_{0:k-1}) = \frac{p(\mathbf{y}_k|\mathbf{x}_k, \mathbf{p}^y_{k-1})\; p(\mathbf{x}_k \,|\, \mathbf{y}_{1:k-1}, \mathbf{u}_{0:k-1}, \mathbf{p}_{0:k-1})}{\int p(\mathbf{y}_k|\mathbf{x}_k, \mathbf{p}^y_{k-1})\; p(\mathbf{x}_k \,|\, \mathbf{y}_{1:k-1}, \mathbf{u}_{0:k-1}, \mathbf{p}_{0:k-1})\, d\mathbf{x}_k}\;, \tag{12}$$

  which is the posterior distribution incorporating the observation information $\mathbf{y}_k$. As for the transition probability, the measurement $\mathbf{y}_k$ is conditionally independent on the observation and control history, thus those terms disappear in the observation likelihood $p(\mathbf{y}_k|\mathbf{x}_k, \mathbf{p}^y_{k-1})$.

Hence, the generic transition function $\mathcal{T}$ in Equation (3b) has the following two-step form in the stochastic shooting transcription:

$$\mathcal{T}\big(\,\mathbf{X}_{k-1},\, \mathbf{D}_{k-1},\, \mathcal{E}_k,\, \mathbf{u}_{k-1},\, \mathbf{p}_{k-1}\big) = \begin{cases} \mathbf{X}^-_k = \mathcal{T}_{predict}\big(\,\mathbf{X}_{k-1},\, \mathbf{D}_{k-1},\, \mathbf{u}_{k-1},\, \mathbf{p}^x_{k-1}\big) \\ \mathbf{X}_k \;= \mathcal{T}_{update}\big(\,\mathbf{X}^-_k,\, \mathcal{E}_k,\, \mathbf{p}^y_{k-1}\big)\;. \end{cases} \tag{13}$$

One interesting feature of the belief formulation is that, while the system point-wise state would dynamically evolve through a one-to-many relationship in a standard MDP, the belief state of the BMDP evolves through the prediction and update steps according to a one-to-one relationship.

Being the uncertain parameters partitioned as $\mathbf{D} = \big[\mathbf{D}_0,\, \mathbf{D}_1,\, \ldots, \mathbf{D}_{N-1}\big]$, the main advantage of the shooting scheme is that it decouples the uncertainty in the different sub-intervals $[t_k, tk+1)$. When the belief is propagated from t_k to t_{k+1}, the stochastic dimensionality is $n_{\xi_k} = n_x + n_{d_k}$, where n_x and n_{d_k} are respectively the state and uncertain parameters $\mathbf{D}_k$ dimensionality, instead of being the total $n_\xi = n_x + n_d$ as it would be with a vanilla Monte Carlo approach. This efficient decoupling avoids the accumulation of uncertainty and the growth of the belief stochastic dimension in time, thus helping containing the curse of dimensionality typical of uncertainty quantification problems. This feature is computationally crucial for an uncertainty quantification method which is called within an optimisation loop numerous times.

A. Navigation Analysis Approach

Treating observations in offline trajectory optimisation is a tricky task. Indeed, a measurement is a random function of the true state of the system and sensor noise, which is however unknown at the time of offline planning. Therefore, simulating a specific observation value $\mathbf{y}_k$, and its corresponding likelihood, rather than another value, is an arbitrary choice corresponding to an arbitrary reduction in the state uncertainty (through the *update* equations). This problem is depicted in Figure 1, where a single observation reduces the uncertainty dispersion.

While reducing the uncertainty is the goal of orbit determination in the operational life of a spacecraft, that is when real measurements are available, when performing robust trajectory optimisation this simulation approach leads to discarding entirely feasible regions of uncertainty.

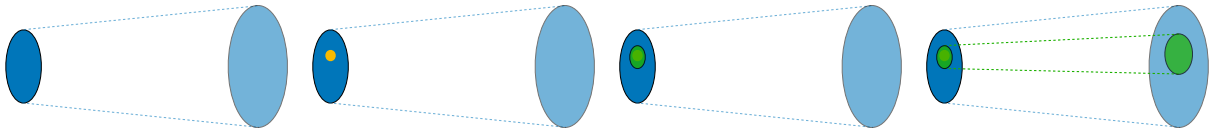

Fig. 1 Effect of single measurement simulation on the uncertainty propagation process. The leftmost frame is the uncertainty propagation without any observation. The second frame indicates the generation of a single observation. The third one shows the uncertainty update of the belief $\mathbf{X}_k$ given the new observation. The rightmost is the new belief propagation after the new observation has been processed.

In navigation analysis, this problem is often dealt with a Monte Carlo simulation over the possible observation space, where for each of the drawn M observation samples $\mathbf{y}_k^{(j)}, j = 1, \ldots, M$, an inference step is performed. This results in a set of possible posterior beliefs

$$\mathbf{X}_k^{(j)} \sim P_{\mathbf{X}_k^{(j)}} = p\left(\mathbf{x}_k \,|\, \mathbf{y}_{1:k}^{(j)}, \mathbf{u}_{0:k-1}, \mathbf{p}_{0:k-1}\right), \tag{14}$$

each resulting from a different observation realisation. In the developed formulation, this procedure corresponds to having different belief states at time t_k.

Such scenario is depicted in Figure 2, where multiple belief components are generated as a consequence of the Monte Carlo samples over the observation space. With this approach, each sample represents a possible realisation of

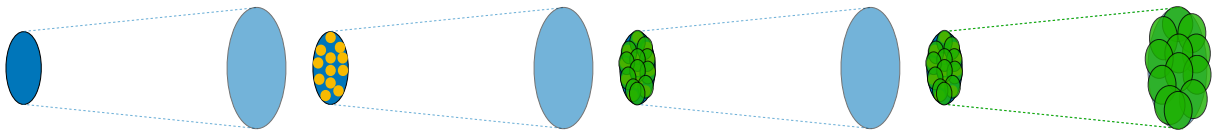

Fig. 2 Effect of Monte Carlo measurement simulation on the uncertainty propagation process. The leftmost frame is the uncertainty propagation without any observation. The second one indicates the generation of a multiple observation samples by Monte Carlo. The third frame shows the multiple uncertainty updates of the belief $\mathbf{X}_k$ given the Monte Carlo observation samples. The rightmost is the belief components propagation after the new observations have been processed.

the operational life of the spacecraft. That is, when the satellite is actually flying and observations are taken, the updated distribution would be one sample out of the multiple green ones (Figure 2). In such a way, when enough observation samples are employed, no uncertainty region is arbitrarily discarded in this offline optimisation, while still each sample have a reduced dispersion as result of the orbit determination process. In addition, each belief component can now evolve according to a belief-specific control, therefore further enabling the modelling of controllers within the developed approach.

In navigation analysis, each component is generally treated as an independent sample to then compute a statistical quantity of interest for the output of the transcription. On the contrary, an advantageous feature of the developed belief formulation when employing a navigation analysis approach is that a single posterior belief can be recovered. Indeed, a belief $\mathbf{X}_k$ can be written as convex combination which summarises the set of M belief components, resulting from different instances of the observation space, as

$$\begin{aligned} \mathbf{X}_k &= \sum_{j=1}^{M} b^{(j)}\, \mathbf{X}_k^{(j)} \sim \sum_{j=1}^{M} b^{(j)}\, P_{\mathbf{X}_k}^{(j)} \\ &\sum_{j=1}^{M} b^{(j)} = 1\,, \end{aligned} \tag{15}$$

where $b^{(j)}$ is the *belief degree*, a weight quantifying the relative degree of likeliness of each $P_{\mathbf{X}_k}^{(j)}$ depending on the observation Monte Carlo sampling. Hence, the advantage of the convex combination is that we can control the posterior components $P_{\mathbf{x}_k}^{(j)}$ singularly through a belief-dependent policy, while at the same time retaining a formal single belief

$P_{\mathbf{x}_k}$ as a mixture, which can be used as general representation of the state uncertainty to evaluate the cost and constraints functions.

From a theoretical standpoint, this operation can be seen as a sampled-base approximation of the marginalisation over all the possible values of the observations, which, when leaving out the actions for ease of notation, is defined as

$$p(\mathbf{x}_k) = \int_{\mathcal{Y}} p(\mathbf{x}_k|\mathbf{y}_k)\, p(\mathbf{y}_k)\, d\mathbf{y}_k \approx \sum_{j=1}^{M} b^{(j)} p(\mathbf{x}_k|\mathbf{y}_k^{(j)}) \,, \tag{16}$$

where $b^{(j)}$ are quadrature (or Monte Carlo) weights. This makes sense because, at the moment of trajectory planning, the only information available is about the expected accuracy of the future measurement, i.e. its likelihood distribution, but not the measurement value itself.

One could, therefore, wonder why to retain the multiple posteriors $P_{\mathbf{x}_k}^{(j)}$ rather than using the single marginalized distribution. The rationale behind preferring the multiple posteriors lays in the actual operational side of a space mission. Indeed, during the operational lifetime of the satellite, one specific measurement value $\bar{\mathbf{y}}_k$ will be received and used to process the state distribution to obtain a single posterior $\bar{P}_{\mathbf{X}_k} = p(\mathbf{x}_k|\bar{\mathbf{y}}_k)$. From it, the control profile will be updated to reflect the updated posterior state knowledge. Hence, it makes sense, conceptually and practically, to retain multiple posteriors, and define a control policy which depends on the belief component.

Another interesting justification for Equation (15) stems from the concept of Jeffrey conditionalisation [22]. This conditionalisation rule describes how the probability of an event A updates given the occurrence of other events $B^{(j)}$ with confidence belief degrees $b^{(j)}$, as

$$\Pr\left(A \mid B^{(1)} \equiv b^{(1)}, \ldots, B^{(M)} \equiv b^{(M)}\right) = \sum_{j} b^{(j)} \Pr\left(A \mid B^{(j)}\right) \,, \tag{17}$$

when the condition events form a partition. This conditionalisation generalises the traditional conditional probability measure, which is now a special case when event $B^{(j)}$ has been observed with certainty, i.e. when its belief degree is $b^{(j)} = 100\%$, and therefore the belief degree of its conjugate is zero. Given this probability measure, we can interpret the belief in Equation (15) as an overall inference step by Jeffrey conditionalisation over sampled observations $\mathbf{y}_k^{(j)}$ with belief degrees $b^{(j)}$:

$$P_{\mathbf{X}_k} = P\big(\mathbf{x}_k \mid \mathbf{y}_k^{(1)} \equiv b^{(1)}, \ldots, \mathbf{y}_k^{(M)} \equiv b^{(M)}\big) = \sum_{j=1}^{M} b^{(j)}\, P\big(\mathbf{x}_k|\mathbf{y}_k^{(j)}\big) = \sum_{j=1}^{M} b^{(j)}\, P_{\mathbf{x}_k}^{(j)} \,. \tag{18}$$

The problem is that, in general, the sampled observations do not form a partition of the observation space which is indeed continuous. However, we can approximate any continuous distribution as a probability mass function by using samples drawn from the original one and the Dirac delta function as [21]

$$p(\boldsymbol{\xi}) \approx \sum_{j=1}^{M} b^{(j)} \delta\big(\boldsymbol{\xi} - \boldsymbol{\xi}^{(j)}\big) \,. \tag{19}$$

If such approximation is introduced for the observation likelihood, then the Jeffrey conditionalisation provides a key formal interpretation of the employed inference step with different sampled measurements for the navigation analysis approach considered.

B. Polynomial Navigation Analysis

Propagating the belief state in time is the most computationally intensive step of the call to the transcription as it requires to solve the Chapman-Kolgomorov equation which has no closed-form solution in the general nonlinear case. Furthermore, when several belief components are present, each of them require a separate solution of the integral in Equation (11). Therefore, in navigation analysis some approximations are typically introduced to speed up the uncertainty propagation. Among them, the most widely used are:

- *Gaussian uncertainty*: $P_{\mathbf{X}_k} = \mathcal{N}\left(\mathbf{X}_k; \boldsymbol{\mu}_{x_k}, \mathbf{P}_{x_k}\right)$
  only the first two moments of the belief state are retained and the normal distribution is assumed as underlying parametric density function;

- *Linear Dynamics*: $F^k_{k-1}(\mathbf{x}_{k-1}) \approx \mathbf{\Phi}^k_{k-1}\,\mathbf{x}_{k-1}$
  the dynamics is linearised around the nominal trajectory, and the state transition matrix $\mathbf{\Phi}^k_{k-1}$ is employed for propagation;
- *Linear Observation Model*: $h_k(\mathbf{x}_k) \approx H_k\,\mathbf{x}_k$
  the observation model is linearised around the nominal state to have a linear mapping between the state and the measurement space.

When these approximations are enforced, the mean and covariance of each belief component are propagated in time with inexpensive matrix multiplications. Furthermore, as the observation model is linearised, the uncertainty update at observation times in Equation (12) reduces to the simple analytical linear Kalman Filter update. These common approximations enable the use of a high number of Monte Carlo samples to the expenses, however, of losing accuracy in the uncertainty propagation process.

In this paper, instead, an approach based on polynomial expansion is employed for efficient and accurate uncertainty propagation. Consider the set $\Omega_{\boldsymbol{\xi}_{k-1}}$ of all possible uncertainty realisations $\boldsymbol{\xi}_{k-1} = [\mathbf{x}_{k-1}, \mathbf{d}_{k-1}]$ at time t_{k-1}, and the set of compatible states at time t_k defined as

$$\mathcal{F}_k = \{F^k_{k-1}(\boldsymbol{\xi}_{k-1}) \,|\, \boldsymbol{\xi}_{k-1} \in \Omega_{\boldsymbol{\xi}_{k-1}}\}\,, \tag{20}$$

where F^k_{k-1} is the numerical mapping as defined in Equation (2). The ultimate goal is to construct a polynomial mapping which maps the stochastic set $\Omega_{\boldsymbol{\xi}_{k-1}}$ to the state set $\mathcal{F}_k$. It is importance to notice that no assumption is done on the distribution of $\boldsymbol{\xi}_{k-1}$, thus the interest lays in constructing an approximation which has good global accuracy over all the set $\Omega_{\boldsymbol{\xi}_{k-1}}$.

The numerical mapping can be expanded in an infinite polynomial series as [23, 24]

$$F^k_{k-1}(\boldsymbol{\xi}_{k-1}) = \sum_{i=0}^{\infty} \alpha_{k,i}\,\Psi_i(\boldsymbol{\xi}_{k-1}) \quad \forall \boldsymbol{\xi}_{k-1} \in \Omega_{\boldsymbol{\xi}_{k-1}}\,, \tag{21}$$

where Ψ_i is the $i\text{-}th$ multivariate polynomial basis and $\alpha_{k,i}$ its coefficient. For practical applications, this expansion is truncated to a finite order q and only the first N_q components retained as

$$F^k_{k-1}(\boldsymbol{\xi}_{k-1}) \approx \widetilde{F}^k_{k-1}(\boldsymbol{\xi}_{k-1}) = \sum_{i=0}^{N_q} \alpha_{k,i}\,\Psi_i(\boldsymbol{\xi}_{k-1})\,, \tag{22}$$

where N_q depends on the choice of the multivariate polynomial space. The coefficients of the polynomial mapping can be computed in numerous ways, e.g. intrusive or non-intrusive methods, by least square or quadrature rules, and so on.

In the current development of this transcription, the stochastic collocation approach is employed [25]: the original function F^k_{k-1} is evaluated (numerical propagation) on a set of collocation points $\boldsymbol{\xi}^{(j)}_{k-1}$, which form the sparse grid, and the response values used to construct the global polynomial approximation $\widetilde{F}^k_{k-1}$ over the entire set of interest. Because the stochastic dimension n_{ξ_k} of $\boldsymbol{\xi}_k$ can be rather high in space applications, the Smolyak polynomial space variant is used to limit the growth of collocation points with n_{ξ_k}, and further fight the curse of dimensionality. The difference in number of collocation points for grids constructed by full tensor product and by sparse Smolyak rule can be seen in Figure 3 for two-dimensional grids constructed with 17 nodes per dimension. Such difference further grows with the number of stochastic dimensions. In this work, Chebyshev polynomials will be used as basis functions Ψ_i of the expansion, hence Clenshaw–Curtis collocation points (Chebyshev extrema) form the sparse grid.

There are several advantages of this sparse polynomial mapping by stochastic collocation over other methods for uncertainty propagation in trajectory optimisation applications:

- being a non-intrusive method, the dynamical model is called as a black-box function, thus pre-existing libraries can be easily interfaced with such transcription without alteration;
- the accuracy of the approximation in Equation (22) can be made as good as desired by increasing the degree q of the polynomial space; the growth of the number of collocation points with the degree q is limited by the sparse Smolyak variant;
- Chebyshev polynomials are employed for their global convergence properties over a compact set [24] and previous applications in a number of aerospace cases [11, 26, 27].

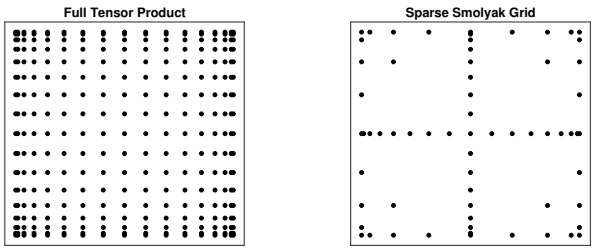

Fig. 3 Comparison of two-dimensional grids constructed by full tensor product (left) or sparse Smolyak rule (right) of one-dimensional grids with 17 collocation points.

The constructed polynomial mapping in Equation (22) is therefore used to speed up the uncertainty propagation step in place of the original numerical propagation, consequently enabling the practical usage of a high number of Monte Carlo samples for the observation sampling (see Section III.A).

C. Practical Approach

Several approaches can be employed to transcribe the OCPUU (3). Among the possible solutions, this section presents two approaches for the practical transcription computation which fits the sequential nature of the employed shooting scheme. Specifically, Section III.C.1 shows the scheme to employ in the most general case of random variables with no specific parametric distribution, whereas Section III.C.2 presents a specialised approach which more efficiently transcribes the OCPUU when the involved uncertainty distributions are assumed Gaussian, which is often the case in navigation analysis.

1. General Case

When no specific assumption or parameterisation is imposed on the stochastic distributions $P(\cdot)$, the equations in Problem (3) have no closed-form solution and numerical techniques are required. In this case, Monte Carlo sampling techniques can be extensively employed to compute the belief transition, objective and constraints mappings for the OCPUU given the availability of inexpensive polynomial mappings.

The prediction and update steps of the belief transition function, in Equation (13), can be computed with the particle filter [21], a sequential Monte Carlo method that approximates the posterior density function as a discrete one by using samples $\mathbf{x}_k^{(i)}$, drawn from a proposal importance distribution $\pi\left(\mathbf{x}_k \mid \mathbf{x}_{k-1}, \mathbf{y}_{1:k}, \mathbf{u}_{0:k-1}, \mathbf{p}_{0:k-1}\right)$, as

$$P_{\mathbf{X}_k} = p(\mathbf{x}_k \mid \mathbf{y}_{1:k}, \mathbf{u}_{0:k-1}, \mathbf{p}_{0:k-1}) \approx \sum_{i=1}^{N} w_k^{(i)}\, \delta\left(\mathbf{x}_k - \mathbf{x}_k^{(i)}\right), \tag{23}$$

where $\delta(\cdot)$ is the Dirac function, and the weights $w_k^{(i)}$ are updated sequentially as

$$w_k^{(i)} = w_{k-1}^{(i)}\, \frac{p(\mathbf{y}_k \mid \mathbf{x}_k^{(i)}, \mathbf{p}_{k-1}^{y})\; p(\mathbf{x}_k^{(i)} \mid \mathbf{x}_{k-1}^{(i)}, \mathbf{u}_{k-1}, \mathbf{p}_{k-1}^{x})}{\pi\left(\mathbf{x}_k^{(i)} \mid \mathbf{x}_{k-1}^{(i)}, \mathbf{y}_{1:k}, \mathbf{u}_{0:k-1}, \mathbf{p}_{0:k-1}\right)}, \tag{24}$$

to account for the received observations and the known dynamical evolution. The main motive behind the particle filter approach is that drawing samples directly from the posterior distribution $P_{\mathbf{X}_k}$ is an unattainable task, whereas evaluating their density value is relatively easy thanks to Equation (12). Therefore, the samples are drawn from a proposal distribution π, whose support should be larger than the posterior one, and then corrective weights are employed to target the posterior distribution $P_{\mathbf{X}_k}$.

The accuracy of the discrete approximation and the particle filter performance greatly depend on the number of particles used, which is further critical for high-dimensional nonlinear problems like navigation analysis for space trajectory. Therefore, the polynomial mapping $\widetilde{F}_{k-1}^{k}$ constructed in the previous section results crucial in this scheme as it allows one to employ a larger number of samples, which can be propagated through an inexpensive polynomial evaluation.

For the Monte Carlo navigation analysis approach, the same particle filter scheme can be applied just running a single update step for each observation sample, and approximating the posterior as a convex combination of the resulting posterior components. Hence, the updated posterior can be written as

$$\begin{aligned} P_{\mathbf{X}_k} = \sum_{j=1}^{M} b^{(j)}\, P_{\mathbf{X}_k}^{(j)} &= \sum_{j=1}^{M} b^{(j)}\, p(\mathbf{x}_k \mid \mathbf{y}_{1:k}^{(j)}, \mathbf{u}_{0:k-1}, \mathbf{p}_{0:k-1}) \\ &\approx \sum_{j=1}^{M} b^{(j)} \sum_{i=1}^{N} w_k^{(i,j)}\, \delta\big(\mathbf{x}_k - \mathbf{x}_k^{(i,j)}\big)\ , \end{aligned} \tag{25}$$

where $\mathbf{x}_k^{(i,j)} \sim \pi\left(\mathbf{x}_k \mid \mathbf{x}_{k-1}, \mathbf{y}_{1:k}^{(j)}, \mathbf{u}_{0:k-1}, \mathbf{p}_{0:k-1}\right)$ have been drawn (propagated) from the proposal distribution that, in the general case, may be chosen to depend on the particular belief component, i.e. $\mathbf{y}_{1:k}^{(j)}$.

Once the belief state is propagated and approximated as in Equation (23), the value of the objective index C and constraints G, which return a statistical quantity of interest given the belief state, can be easily estimated by the N samples $\mathbf{x}_k^{(i)}$ used for the discrete approximation. As a relevant example, any G (or C) function in the form of an expectation of a generic function ϕ, e.g. expected value constraints, chance constraints, in variance and so on, can be immediately computed as

$$G\big(\mathbf{X}_k\big) = \mathbb{E}\big[\phi\big(\mathbf{X}_k\big) \mid \mathbf{y}_{1:k}\big] \approx \sum_{i=1}^{N} w_k^{(i)} \phi\big(\mathbf{x}_k^{(i)}\big)\ , \tag{26}$$

or similarmly for the case of multiple belief components $\mathbf{X}_k \sim \sum_{j=1}^{M} b^{(j)} P_{\mathbf{X}_k}^{(j)}$, as in Equation (25), the integral is

$$G\big(\mathbf{X}_k\big) = \mathbb{E}\big[\phi\big(\mathbf{X}_k\big) \mid \mathbf{y}_{1:k}\big] \approx \sum_{j=1}^{M} b^{(j)} \sum_{i=1}^{N} w_k^{(i,j)} \phi\big(\mathbf{x}_k^{(i,j)}\big)\ . \tag{27}$$

This particle filter-based approach to the practical computation of the shooting transcription should be employed in the most general case of non-Gaussian uncertainty, nonlinear dynamical system and observation model. This concludes the transcription method for the OCPUU as formulated in Equation (3).

In the next section, a Gaussian tailored approach is presented to more efficiently tackle the common case of optimal control problems under Gaussian-assumed uncertainty.

2. Gaussian Case

A special case, of particular interest for spacecraft navigation analysis applications, is the one where all the involved uncertainty distributions are Gaussian:

$$\mathbf{X}_0 \sim \mathcal{N}\left(\mathbf{X}_0;\, \boldsymbol{\mu}_{X_0}, \mathbf{P}_{X_0}\right) \tag{28a}$$

$$\mathbf{D} \sim \mathcal{N}\left(\mathbf{D};\, \boldsymbol{\mu}_{D}, \mathbf{P}_{D}\right) \tag{28b}$$

$$\mathbf{Y}_k|\mathbf{x}_k \sim \mathcal{N}\left(\mathbf{Y}_k|\mathbf{x}_k;\, \boldsymbol{\mu}_{Y_k}, \mathbf{P}_{Y_k}\right) \tag{28c}$$

$$\mathbf{X}_k \sim \mathcal{N}\left(\mathbf{X}_k;\, \boldsymbol{\mu}_{X_k}, \mathbf{P}_{X_k}\right)\ , \tag{28d}$$

where $\mathbf{m}$ indicates the mean and $\mathbf{P}$ the covariance of the normal distributions. The distributions in Equations (28a-c) are Gaussian by construction, while the belief state in Equation (28d) is approximated as Gaussian.In this case, dedicated methods exist to efficiently compute each quantity in Problem (3), which are more suitable than general Monte Carlo methods for Gaussian distributions.

As for the prediction and update steps in the belief transition Equation (13), the *Gaussian assumed density filter* [28] can be applied, whose main idea is to approximate the propagated and the posterior distributions as Gaussian ones, that is only computing and retaining the first two moments. With this sequential filtering scheme, the two-step belief transition becomes:

- $\mathbf{X}_k^- = \mathcal{T}_{predict}\left(\mathbf{X}_{k-1}, \mathbf{D}_{k-1}, \mathbf{u}_{k-1}, \mathbf{p}_{k-1}^x\right)$ the predicted distribution is written as

$$\mathbf{X}_k^- \sim \mathcal{N}\left(\mathbf{X}_k^-;\, \boldsymbol{\mu}_{X_k^-}, \mathbf{P}_{X_k^-}\right)\ , \tag{29}$$

with mean and covariance given by

$$\begin{aligned}\boldsymbol{\mu}_{X_k^-} &= \int \widetilde{F}_{k-1}^{k}(\mathbf{z}_{k-1}^-, \mathbf{u}_{k-1}, \mathbf{p}_{k-1}^x)\ \mathcal{N}\big(\mathbf{z}_{k-1}^-\,;\,\boldsymbol{\mu}_{Z_{k-1}^-}, \mathbf{P}_{Z_{k-1}^-}\big)\, d\mathbf{z}_{k-1}^- \\ \mathbf{P}_{X_k^-} &= \int \big(\widetilde{F}_{k-1}^{k}(\mathbf{z}_{k-1}^-, \mathbf{u}_{k-1}, \mathbf{p}_{k-1}^x) - \boldsymbol{\mu}_{X_k^-}\big)\big(\widetilde{F}_{k-1}^{k}(\mathbf{z}_{k-1}^-, \mathbf{u}_{k-1}, \mathbf{p}_{k-1}^x) - \boldsymbol{\mu}_{X_k^-}\big)^T \mathcal{N}\big(\mathbf{z}_{k-1}^-\,;\,\boldsymbol{\mu}_{Z_{k-1}^-}, \mathbf{P}_{Z_{k-1}^-}\big)\, d\mathbf{z}_{k-1}^- \,,\end{aligned} \tag{30}$$

where $\mathbf{Z}_{k-1}^- = [\mathbf{X}_{k-1}, \mathbf{D}_{k-1}]^T$ is the joint random variable of the uncertain state and model parameters.

- $\mathbf{X}_k = \mathcal{T}_{update}\big(\mathbf{X}_k^-, \mathcal{E}_k, \mathbf{p}_{k-1}^y\big)$ the posterior distribution after receiving an observation $\mathbf{y}_k$ is

$$\mathbf{X}_k \sim \mathcal{N}\left(\mathbf{X}_k; \boldsymbol{\mu}_{X_k}, \mathbf{P}_{X_k}\right), \tag{31}$$

with mean and covariance

$$\begin{aligned}\boldsymbol{\mu}_{X_k} &= \boldsymbol{\mu}_{X_k}^- + \mathbf{K}_k(\mathbf{y}_k - \boldsymbol{\mu}_{Y_k}) \\ \mathbf{P}_k &= \mathbf{P}_k^- - \mathbf{K}_k \mathbf{S}_k \mathbf{K}_k^T \,.\end{aligned} \tag{32}$$

The observation mean $\boldsymbol{\mu}_{Y_k}$ and Kalman gain $\mathbf{K}_k$ are computed as

$$\begin{aligned}\boldsymbol{\mu}_{Y_k} &= \int h(\mathbf{z}_k, \mathbf{p}_{k-1}^y)\, \mathcal{N}\big(\mathbf{z}_k\,;\,\boldsymbol{\mu}_{Z_k}, \mathbf{P}_{Z_k}\big)\, d\mathbf{z}_k \\ \mathbf{S}_{Y_k} &= \int \big(h(\mathbf{z}_k, \mathbf{p}_{k-1}^y) - \boldsymbol{\mu}_{Y_k}\big)\big(h(\mathbf{z}_k, \mathbf{p}_{k-1}^y) - \boldsymbol{\mu}_{Y_k}\big)^T \mathcal{N}\big(\mathbf{z}_k\,;\,\boldsymbol{\mu}_{Z_k}, \mathbf{P}_{Z_k}\big)\, d\mathbf{z}_k \\ \mathbf{C}_{XY_k} &= \int \big(\mathbf{x}_k - \boldsymbol{\mu}_{X_k}^-\big)\big(h(\mathbf{z}_k, \mathbf{p}_{k-1}^y) - \boldsymbol{\mu}_{Y_k}\big)^T \mathcal{N}\big(\mathbf{z}_k\,;\,\boldsymbol{\mu}_{Z_k}, \mathbf{P}_{Z_k}\big)\, d\mathbf{z}_k \\ \mathbf{K}_k &= \mathbf{C}_{XY_k}\, \mathbf{S}_{Y_k}^{-1} \,,\end{aligned} \tag{33}$$

where $\mathbf{Z}_k = [\mathbf{X}_k, \mathcal{E}_k]^T$ is the joint random variable of the uncertain state and sensor noise, $\mathbf{S}_{Y_k}$ is the observation covariance, whereas $\mathbf{C}_{XY_k}$ is the cross covariance between state and observation.

Hence, both the prediction and update steps of the belief transition function can be reduced to the computation of the expected value of a generic function ϕ, that is the function integral with Gaussian density distribution as weighting function as

$$\mathbb{E}[\phi(\mathbf{Z})] = \int \phi(\mathbf{z})\, \mathcal{N}\big(\mathbf{z}\,;\,\boldsymbol{\mu}_Z, \mathbf{P}_Z\big)\, d\mathbf{z} \,. \tag{34}$$

Integrals of this type can be solved with a variety of well established numerical techniques. To optimally exploit simultaneously the Gaussian nature of such integral and the constructed polynomial mapping $\widetilde{F}_{k-1}^{k}$, the sample-based Gauss-Hermite scheme is employed to compute such integrals with a multi-dimensional cubature rule as

$$\int \phi(\mathbf{z})\, \mathcal{N}\big(\mathbf{z}\,;\,\boldsymbol{\mu}_Z, \mathbf{P}_Z\big)\, d\mathbf{z} \approx \sum_{i=1}^{N} w^{(i)}\, \phi\left(\mathbf{z}^{(i)}\right), \tag{35}$$

where $\mathbf{z}^{(i)}$ are the roots of the multivariate Hermite polynomial and $w^{(i)}$ the corresponding weights.

The advantage of this approach over similar sample-based ones, e.g. Unscented Transform, is that the estimation fidelity can be made as accurate as desired simply using more quadrature points, that is a higher order Hermite polynomial. A high accuracy computation of the integrals in Equation (30) is made possible by the Chebyshev polynomial mapping $\widetilde{F}_{k-1}^{k}$, which can be employed to propagate a great number of samples inexpensively.

The multivariate Gauss-Hermite grid is usually constructed by Cartesian products of univariate ones. In order to alleviate the curse of dimensionality encountered in high-dimensional problems, like the ones tackled in navigation analysis, a sparse Gauss-Hermite version is employed to contain the number of samples for high stochastic dimensions [25].

The Gaussian assumed density formulation in expectation in still applies to the case of belief state represented as sum of belief components because of the linearity property of the integral operator. Indeed, if the probability density function is a convex combination of probability components as

$$\mathcal{N}\big(\mathbf{Z}\,;\,\boldsymbol{\mu}_Z, \mathbf{P}_Z\big) = \sum_{j=1}^{M} b^{(j)} \mathcal{N}\big(\mathbf{Z}\,;\,\boldsymbol{\mu}_Z^{(j)}, \mathbf{P}_Z^{(j)}\big) \tag{36}$$

then the generic integral in Equation (34) becomes

$$\begin{aligned}\int \phi(\mathbf{z})\, \mathcal{N}\big(\mathbf{z}\,;\, \boldsymbol{\mu}_Z, \mathbf{P}_Z\big)\, d\mathbf{z} &= \int \phi(\mathbf{z}) \sum_{j=1}^{M} b^{(j)} \mathcal{N}\big(\mathbf{Z}\,;\, \boldsymbol{\mu}_Z^{(j)}, \mathbf{P}_Z^{(j)}\big)\, d\mathbf{z} = \\ &= \sum_{j=1}^{M} b^{(j)} \int \phi(\mathbf{z})\, \mathcal{N}\big(\mathbf{Z}\,;\, \boldsymbol{\mu}_Z^{(j)}, \mathbf{P}_Z^{(j)}\big)\, d\mathbf{z} \approx \sum_{j=1}^{M} b^{(j)} \sum_{i=1}^{N} w^{(i,j)} \phi\left(\mathbf{z}^{(i,j)}\right),\end{aligned} \tag{37}$$

which is the sum of the expectations with respect to the belief components weighted for the corresponding belief degrees.

It is interesting to notice that both in the case of generic uncertainty tackled with a particle filter, and Gaussian uncertainty solved with a quadrature filter, the end operation to perform is the computation of integrals by sample-based approximations. The formulation is similar for both the cases, indeed Equation (26) is the same as Equation (35) for the single belief representation, and Equation (27) is the same as Equation (37) for the mixture case, where only the weights and samples come from different rules.

3. Epistemic Case

When some of the stochastic variables are modelled with epistemic uncertainty, the epistemic OCPUU requires the computation of bounds (see Equation (9)) on the the constraints and objective functions. Such extrema are computed by means of an optimisation routine which look for the distributions within the imprecise set $\mathcal{P}$ which correspond to the infimum and supremum of the quantity of interest. Therefore, the procedure to solve Problem (10) involves two nested optimisation loops: the outer one operates over the control variables to minimise the objective index and respect the constraints; the inner one works with the epistemic parameters to compute the lower and upper bounds.

For the general case described in Section III.C.1, a generalisation of the particle filter to epistemic uncertainty was developed [29] which employs *importance sampling* to substitute the optimisation over the distributions with an efficient equivalent one over the importance weights. On the other hand, for the Gaussian case solved with a Kalman Filter as in Section III.C.2, the inner optimisation operates over the imprecise set directly, requiring a new transcription call for every evaluation.

In the practical solution of the epistemic case, the polynomial mapping in Equation (22) can be constructed only once per iteration of the outer loop, and the subsequent inner loop optimisation performed exploiting the inexpensive surrogate. This can be done on the basis that, while the outer loop may change significantly the reference trajectory, the inner loop tunes only the stochastic distributions and therefore should still operate in the high-accuracy region of the surrogate.

IV. Test Case: Europa Clipper Robust Optimisation

The problem of optimising the $\Delta V99$ for one leg of the Europa Clipper tour is addressed in this application. The goal is to compute the optimal nominal trajectory which minimises the sum of deterministic and statistical manoeuvres, while respecting desired flyby parameters and a final boundary condition *in expected value*, and having a collision probability after targeting, i.e. *chance constraint*, with Europa below 0.1%.

Therefore, here only one part of the full tour is robustly optimised to meet flight dynamics requirements. The final boundary condition ensures that when the robust modified trajectory is substituted back in the full tour, the spacecraft can actually continue the next legs of the tour according to the original design.

After the description of the applications setup, both the cases of pure aleatoric uncertainty and combined epistemic and aleatoric uncertainty will be addressed in this section.

A. Problem Setup

For this application, the interest lays in finding the optimal *open-loop* control $\Delta\mathbf{v}$ which corresponds to a trajectory which is most robust and reliable to the considered uncertainties. Therefore, the *closed-loop* controllers $\delta\Delta\mathbf{v}$, steering the different samples (belief components), are not optimised but their value is computed by an analytical linear law.

The problem scenario addressed is depicted in Figure 4 in its several phases. Specifically, this is the navigation analysis performed during each optimisation call, i.e. for given $\Delta\mathbf{v}$ controls, represented in green, while the analytical controllers $\delta\Delta\mathbf{v}$ are represented in red. In Figure 4(a), the trajectory starts from the Europa flyby E17 with the initial

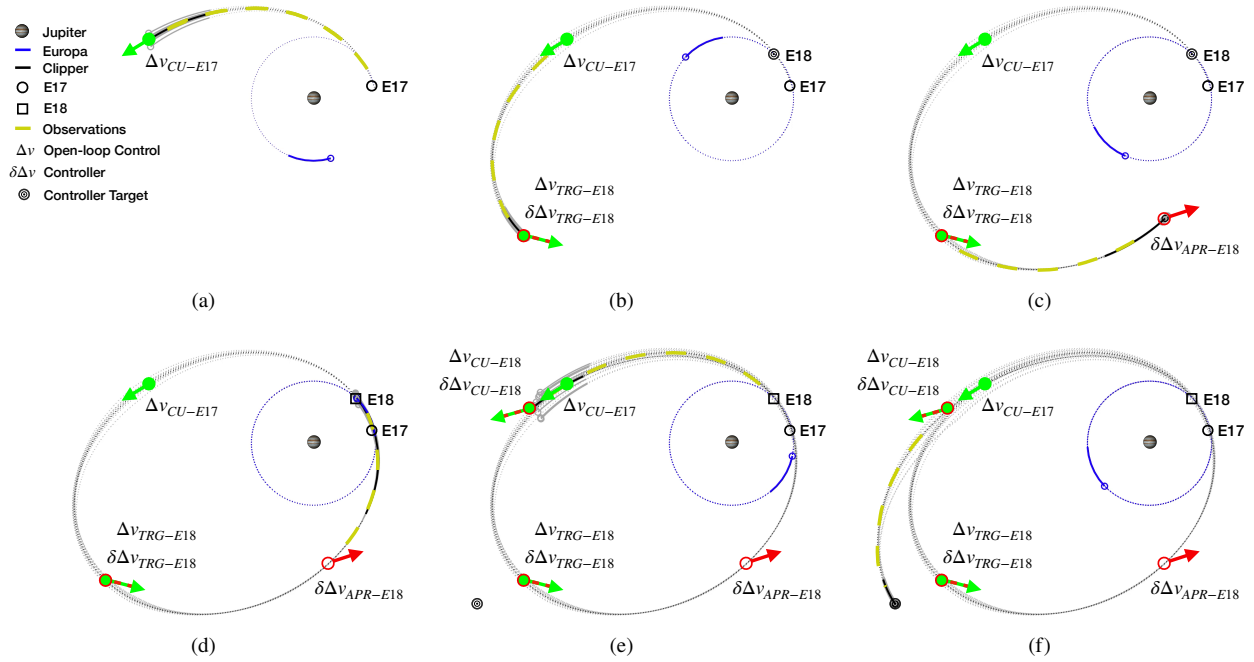

Fig. 4 Schematic representation of navigation analysis setup for part of Europa Clipper leg stochastic optimisation test case.

dispersion $\mathbf{X}_0 \sim P_{\mathbf{X}_0}$. $\mathbf{X}_0$ is propagated to the time of the *clean-up*,which is a post-flyby ($\sim$ 3 days after) maneuver to correct biases as resulting from navigation errors worsened by the previous close encounter. During such propagation, orbit determination campaigns are carried out, represented in yellow, with a 8 hours ON 8 hours OFF schedule (dashed line) to improve the spacecraft trajectory knowledge This 8 hours ON 8 hours OFF pattern is adopted to faithfully model the part-time availability of the DSN tracking network for this mission. The OD stops at a cut-off time before the subsequent maneuver, here set to one day, to model the time needed by the spacecraft operators to compute the updated trajectory. The aforementioned MCNA approach is employed to simulate observation samples and update the belief state until $\mathbf{X}_{CU-E17} \sim \sum_{j=1}^{M} b^{(j)} \mathbf{X}^{(j)}_{CU-E17}$. Hence, the deterministic maneuver $\Delta\mathbf{v}_{CU-E17}$ is applied equally to each belief component.

Then, as in Figure 4(b), the belief state is propagated and updated during OD arcs until $\mathbf{X}_{TRG-E18}$ at the time of *targeting*, close to the trajectory apocenter, when the deterministic $\Delta\mathbf{v}_{TRG-E18}$ is applied to the belief state to target the next Europa flyby E18. The deterministic impulse is combined with a linear analytical controller $\delta\Delta\mathbf{v}^{(j)}_{TRG-E18}$ to correct for the state dispersions and target the desired B-plane conditions (**B** vector and Linearised Time-of-Flight) [30] at E18, with a different velocity correction applied to different belief components $\mathbf{X}^{(j)}_{TRG-E18}$. The belief is then propagated (Figure 4(c)) and observations incorporated until $\mathbf{X}_{APR-E18}$ at the *approach* time, when a pre-flyby ($\sim$ 3 days before) controller $\delta\Delta\mathbf{v}^{(j)}_{APR-E18}$ is enforced to perform final corrections before the forthcoming encounter. Again, this controller applies component-specific impulses to linearly target the desired B-plane conditions for E18.

Figure 4(d) shows the subsequent belief transition until the E18 flyby after the approach maneuver. At E18, the belief state $\mathbf{X}_{E18}$ is used to compute the expected value of the B-plane parameters to impose a constraint with the target conditions in the optimisation loop. In Figure 4(e), the belief is propagated and updated until the next clean-up maneuver, which has both nominal $\Delta\mathbf{v}_{CU-E17}$ and statistical $\delta\Delta\mathbf{v}_{CU-E17}$ components, to accurately target the final position at the next apocenter, as in Figure 4(f). At the final time, the next apocenter in this case, the belief state $\mathbf{X}_N$ is employed to compute a final boundary condition in expected value for the position, and the final velocity mismatch.

The whole trajectory considered lasts 21 days, from E17 to the second apocenter passage. The employed inertial reference frame is the Mean ecliptic and equinox of J2000 one. The motion is described in high-fidelity full-ephemeris dynamics, taking into account the gravitational pull of Jupiter (central and J_2), its moons Europa (central and J_2), Io, Ganymede and Callisto, and the Sun. The dynamics is integrated with the propagation module of the mission design tool jTOP [31].

B. Aleatoric Scenario

1. Aleatoric Uncertainty Model

The initial dispersion is modelled as a Gaussian random variable with covariance $\mathbf{P}_{X_0}$ set as diagonal in the Radial-Transversal-Normal (RTN) frame, with the square root of the diagonal values (standard deviations) as reported in Table 1. This expected dispersion is reconstructed from OD campaigns post-flyby.

The execution errors of the impulsive maneuvers are modelled with Gates' model [32], which decompose the error in magnitude and pointing components. Execution errors are considered on both the nominal $\Delta\mathbf{v}$ and statistical $\delta\Delta\mathbf{v}$ maneuvers.

As for the orbit determination campaigns, the measured quantity is the range and range-rate of the spacecraft with respect to the Earth. The likelihood function is modelled as Gaussian, and its covariance characterizing the observation accuracy is assumed diagonal.

The parameters for these uncertainty models are detailed in Table 1, set in line with values found in previous navigation analysis studies for Europa Clipper [33, 34], which reports respectively the square root of the diagonal values (standard deviations) for the initial dispersion, the Gates' model parameters for the execution errors, and the standard deviation values for the accuracy of each observation type.

Table 1 Parameters of uncertainty models considered in Europa's moon flyby stochastic optimisation. The initial dispersion is expressed in terms of standard deviation of position and velocity in RTN components. The execution error is modelled by Gates' model and the corresponding parameters are reported. The observation noise is expressed in terms of 1-σ accuracy for range and rangerate components.

Uncertainty	Component	Value	
Initial Dispersion	Position (RTN)	[3.7, 5.3, 9.3]	[m]
	Velocity (RTN)	[2.3, 3.4, 5.9]	[mm/s]
Execution Error	Fixed Pointing	3.33	[mm/s]
	Proportional Pointing	6.67	[mrad]
	Fixed Magnitude	4.67	[mm/s]
	Proportional Magnitude	0.33%	[-]
Observation Accuracy	Range	3.0	[m]
	Rangerate	0.1	[mm/s]

2. Aleatoric Belief Stochastic Formulation

Given the scenario introduced in Section IV.A, the problem of optimising the $\Delta V99$ for one leg of the Europa's Clipper tour is framed under the developed stochastic formulation as

$$\min_{\Delta\mathbf{v}_{k1}} \quad \Delta V99 \tag{38a}$$

$$\text{s.t.} \quad \mathbf{X}_k = \mathcal{T}\left(\mathbf{X}_{k-1}, \Delta\mathbf{v}_{k-1}, \mathbf{D}_{k-1}, \mathcal{E}_k\right) \tag{38b}$$

$$Pr_{TRG}\left(R_{E18} \leq R_{EUR}\right) < 0.1\% \tag{38c}$$

$$\mathbb{E}\left[\mathbf{B}_{E18}\right] = \overline{\mathbf{B}}_{E18} \tag{38d}$$

$$\mathbb{E}\left[\mathbf{R}_f\right] = \bar{\mathbf{r}}_f \tag{38e}$$

$$\mathbf{X}_0 \sim \mathcal{N}_{\mathbf{X}_0}\left(\boldsymbol{\mu}_{X_0}, \mathbf{P}_{X_0}\right), \tag{38f}$$

where the index $k1 = \{CU\text{-}E17, TRG\text{-}E18, CU\text{-}E18\}$ is for the *open-loop* deterministic $\Delta\mathbf{v}$s to optimise. The $\Delta V99$ is defined as the ΔV to address 99% of the possible uncertainty realisations, which in this scenario takes the form of

$$\begin{aligned}\Delta V99 = \; & Q_{\Delta V_{CU\text{-}E17}}(0.99) + Q_{\{\Delta V+\delta\Delta V\}_{TRG\text{-}E18}}(0.99) + \\ & Q_{\delta\Delta V_{APR\text{-}E18}}(0.99) + Q_{\{\Delta V+\delta\Delta V\}_{CU\text{-}E18}}(0.99) + Q_{\Delta V_F}(0.99),\end{aligned} \tag{39}$$

where $Q_{(\cdot)}(0.99)$ is the quantile function of the subscript uncertain maneuver evaluated at 99% probability. The *closed-loop* controllers $\delta\Delta\mathbf{v}$ are not optimised, but still contribute to the objective index. ΔV_F is the final velocity mismatch between the final belief and the desired state, and it is taken into account to ensure the spacecraft can optimally continue the rest of the original tour.

Equation (38b) is the belief transition function, with the execution errors modelled in $\mathbf{D}_{k-1}$, which is computed with the Gaussian assumed filtering scheme (see Section III.C.2) in this application as the Gates' model is sampled from a three-dimensional normal distribution. Equation (38c) is the delivered probability of impact after targeting, written as probability of distance at flyby E18 to be smaller or equal to the radius of Europa, to be smaller than 0.1%. This chance constraint is computed after targeting, that is without adding the approach maneuvers, to ensure environmental protection to Europa even in the event of spacecraft loss after the targeting. Equation (38d) requires the expected value of the B-plane flyby conditions to be fixed to a target vector, as well as Equation (38e) imposes the expected value of the final belief to be equal to a final target position vector. Finally, Equation (38f) is the initial belief condition, whose $\mathbf{P}_{X_0}$ is given in Table 1 while the mean $\boldsymbol{\mu}_{X_0}$ comes from the full nominal tour.

3. Aleatoric Robust Optimisation Results

The deterministic optimal solution reported in Table 2 is employed as first guess for the stochastic optimisation. Such solution meets the flyby and final boundary conditions, but violates the chance constraint as the resulting probability of impact is $Pr\big(DCA \leq R_{EUR}\big) = 0.75 \not\leq 0.1\%$.

Table 2 Free variables, $\Delta V99$ and Probability of Impact (PoI) for deterministic solution employed as first guess for stochastic optimisation.

Solution	$\Delta\mathbf{v}_{\text{CU-E17}}$ [m/s]	$\Delta\mathbf{v}_{\text{TRG-E18}}$ [m/s]	$\Delta\mathbf{v}_{\text{CU-E18}}$ [m/s]	Det ΔV [m/s]	$\Delta V99$ [m/s]	$\Delta V99$/Det ΔV [-]	PoI [-]
Deterministic	[0.0 , 0.0 , 0.0]	[−1.30, +2.86, +3.23]	[0.0 , 0.0 , 0.0]	4.51	8.05	1.79	0.75%

A visualization of the probability of impact for such solution is displayed in Figure 5, where the state uncertainty at different moments during the trajectory is propagated to the B-plane without applying successive maneuvers or performing new orbit determination campaigns. The top-left plot shows the delivered B-plane ellipses that would result if the spacecraft was not controlled or observed anymore after the E17 clean-up. The top-right plot shows the B-plane confidence regions delivered after the targeting maneuvers, that is the uncertainty on which the chance constraint for the probability of impact is computed. For this deterministic trajectory, it is possible to see that indeed the 3-σ region has a non-zero intersection with the B-plane equivalent surface of Europa (represented by the thick black line at $h = 0$ km), leading to an unmet PoI requirement. The bottom-left plot displays the B-plane uncertainty propagated without new OD after the approach maneuver, which results notably smaller with respect to the after targeting one because of the new OD arcs and the controller $\delta\Delta V_{\text{APR-E18}}$. The bottom-right plot finally shows the uncertainty at the B-plane as reconstructed using the OD arcs after the approach.

The estimated $\Delta V99$ for the deterministic trajectory is approximately 80% larger than the deterministic one, a cost increase in line with previous navigation analysis for the Europa Clipper trajectory [35].

Starting from this infeasible solution, the goal of the robust optimisation approach is to find the robust optimal trajectory which minimises the $\Delta V99$ while respecting the PoI constraint, and keeping the expected flyby conditions and terminal position fixed. The belief optimal control problem (38) is solved by interfacing the stochastic shooting transcription developed in this paper with the nonlinear programming solver MATLAB's *fmincon*, using the interior-point algorithm.

The stochastic belief optimisation approach found a feasible trajectory respecting the chance constraint below the imposed threshold. Table 3 reports the optimum solution and the statistical quantities of interest for the converged robust trajectory. The value of the constraints in expected value are not included as they are satisfied up to small thresholds.

Table 3 Free variables, $\Delta V99$ and Probability of Impact (PoI) for robust solution optimised with the stochastic belief approach.

Solution	$\Delta\mathbf{v}_{\text{CU-E17}}$ [m/s]	$\Delta\mathbf{v}_{\text{TRG-E18}}$ [m/s]	$\Delta\mathbf{v}_{\text{CU-E18}}$ [m/s]	Det ΔV [m/s]	$\Delta V99$ [m/s]	$\Delta V99$/Det ΔV [-]	PoI [-]
Stochastic	[+0.12, +0.18, +0.09]	[−2.09, +2.01, +1.99]	[−1.21, +0.56, −1.79]	5.98	9.91	1.66	0.09%

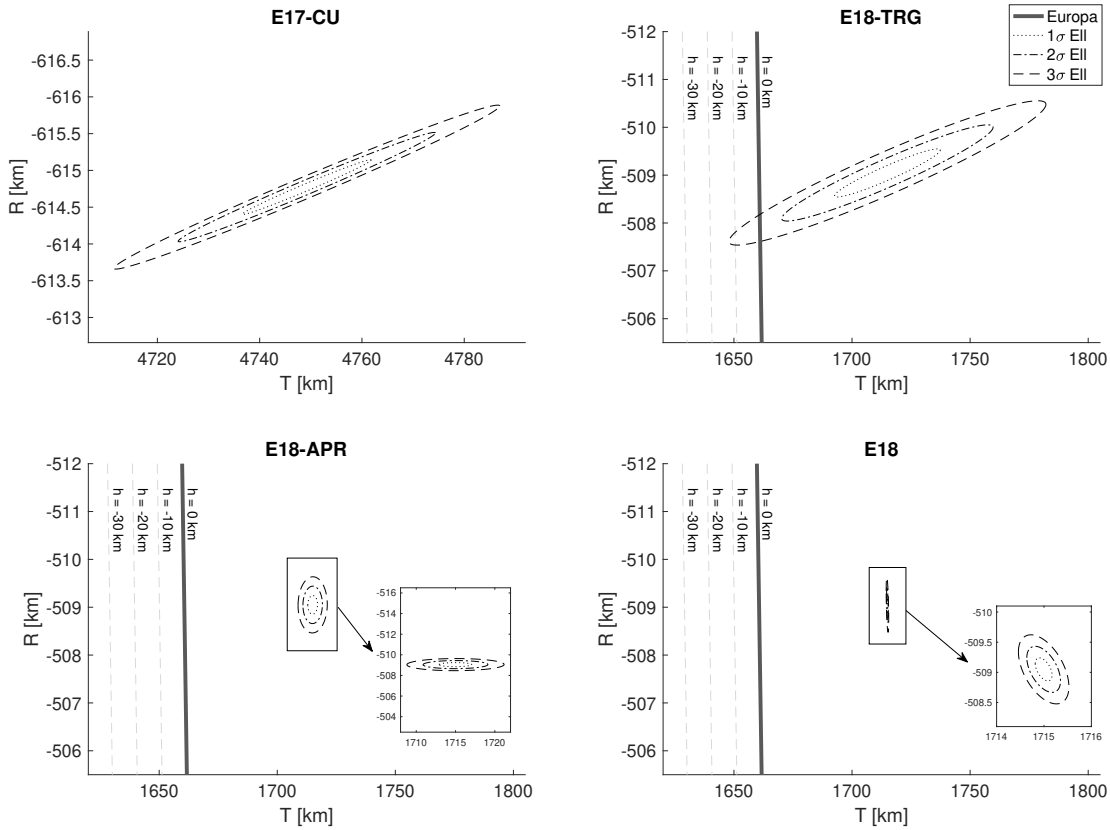

Fig. 5 Spacecraft delivered 1-, 2- and 3-σ confidence ellipses in B-plane parameters as mapped from the state uncertainty at different times along the deterministic trajectory without successive maneuvers and observations as resulting from aleatoric uncertainty.

Looking at the deterministic $\Delta\mathbf{v}$ allocation, one can infer that the feasibility on the PoI constraint were realised by trading off part of the targeting maneuver with the clean-up ones. The execution errors coming from an increased $\Delta\mathbf{v}_{CU-E17}$ can be adjusted by the controller at the apocenter, while the lower $\Delta\mathbf{v}_{TRG-E18}$ and associated execution errors, results in a smaller uncertainty delivered at the B-plane (see in Figure 6). After the flyby, a $\Delta\mathbf{v}_{CU-E18}$ is now needed to return to the target trajectory at the final time.

Overall the optimal trajectory has a higher deterministic ΔV then the first guess, but the infeasibility is restored. We observe that the percentage increase of the statistical $\Delta V99$, with respect to the deterministic ΔV, is now lower, i.e. 66%, indicating that the optimal trajectory can compensate the possible uncertainty realisations more efficiently and robustly.

Figure 6 shows the B-plane delivered uncertainties of the robust trajectory, which are considerably different from the delivered uncertainties of the first guess . The top-right plot of the uncertainty mapped after targeting, used for the PoI computation, shows that the 3-σ confidence ellipse does not cross the equivalent surface of Europa. By comparing it with the corresponding plot in Figure 5, the robust B-plane ellipse has a smaller semi-major axis, which mainly contributes to the PoI, whereas it has a larger semi-minor axis, which has a limited contribution to the PoI constraint. The robust ellipse is also rotated counterclockwise, which leads to an even lower impact probability.

To quickly verify that the increase in the $\Delta V99$ between the robust solution and the first guess is due to the initial infeasibility, a stochastic optimisation has been run removing the PoI constraint and starting from the same initial guess. Table 4 shows the unconstrained optimal solution, with a lower $\Delta V99$ compared to that of the first guess, although the deterministic ΔV is slightly higher. This result further confirms that the stochastic robust optimum differs from the deterministic one, and that the statistical performance are indeed improved.

As done in Figure 6 for key events in the trajectory, the spacecraft state uncertainty can be mapped to B-plane coordinates from any time during the trajectory. Figure 7 provides an insightful visualisation of how the maneuvers and observation arcs affect the flyby uncertainties. In particular, the figure shows (y-axis) the semi-major (SMAA) and

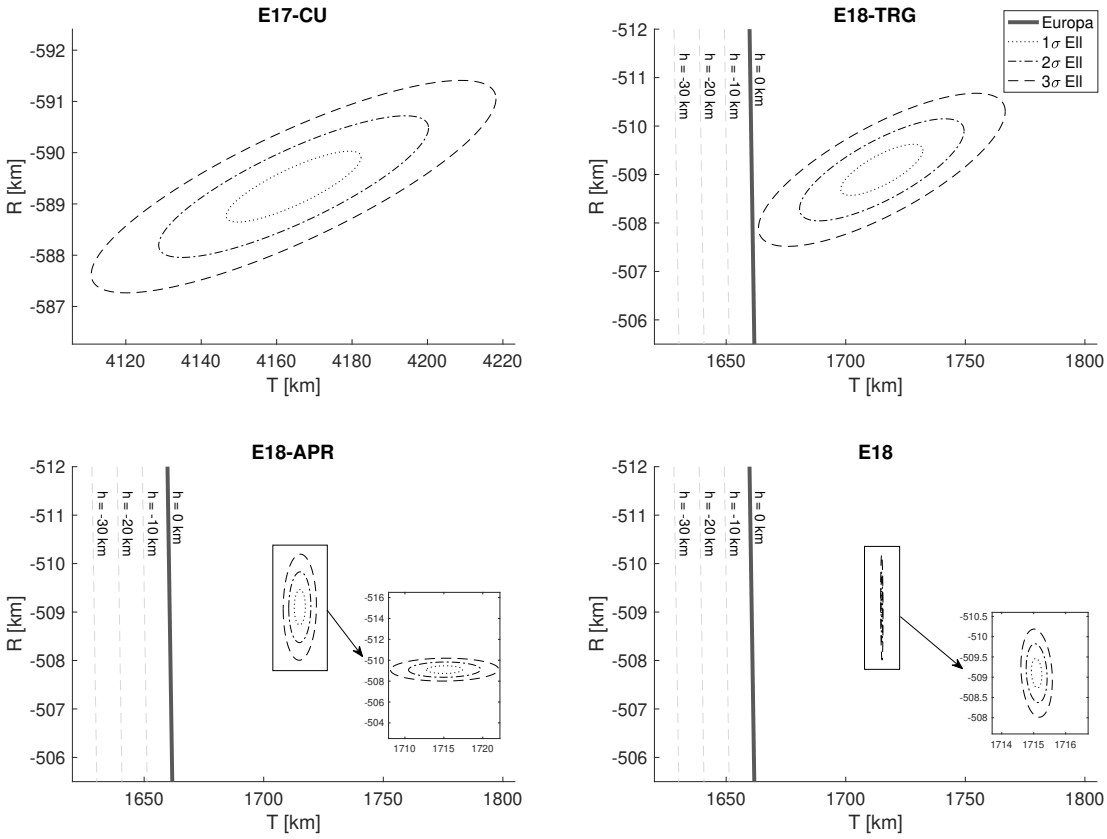

Fig. 6 Spacecraft delivered 1-, 2- and 3-σ confidence ellipses in B-plane parameters as mapped from the state uncertainty at different times along the robust trajectory without successive maneuvers and observations as resulting from aleatoric uncertainty.

Table 4 Free variables, $\Delta V99$ and Probability of Impact (PoI) for verification solution optimised with the stochastic belief approach without imposing the PoI constraint.

Solution	$\Delta\mathbf{v}_{\text{CU-E17}}$ [m/s]	$\Delta\mathbf{v}_{\text{TRG-E18}}$ [m/s]	$\Delta\mathbf{v}_{\text{CU-E18}}$ [m/s]	Det ΔV [m/s]	$\Delta V99$ [m/s]	$\Delta V99$/Det ΔV [-]	PoI [-]
Verification	[0.0 , −0.01, −0.01]	[−1.28, +2.89, +3.25]	[−0.04, −0.02, +0.03]	4.6	8.02	1.74	0.76%

semi-minor (SMIA) axes of the B-plane 1-σ confidence ellipse, i.e. in-plane components, and of the uncertainty in linearised time of closest approach (LTCA), i.e. out-of-B-plane component, as function of different times along the trajectory (x-axis), if no other action is taken after that time (delivered uncertainty).
The value of the mapped uncertainty is around 10 km and 500 m in SMAA and SMIA, and 10 seconds in LTCA, as resulting purely from the initial dispersion as in Table 1. The mapped uncertainty exhibits then a jump at the E17 clean-up maneuver time because of the introduced executions errors. Successively, the orbit determination arcs reduce the B-plane ellipsoid of more than one order of magnitude in SMAA and LTCA, whereas the reduction in SMIA is more modest. The main targeting maneuver and its high execution errors cause a major spike in the delivered uncertainty. The values of SMAA and SMIA at this event are critical for the robust optimisation process, as this B-plane mapped uncertainty is the one employed for the probability of impact computation. Successive OD arcs help reducing significantly the SMAA and LTCA mapped dispersion until another, more contained, jump at the approach maneuver before E18. Finally, the measurements arcs before E18 reduce the mapped uncertainty even further, to have an expected 1-σ uncertainty at flyby of few hundred of meters in SMAA and SMIA, and few tens of ms for the LTCA.

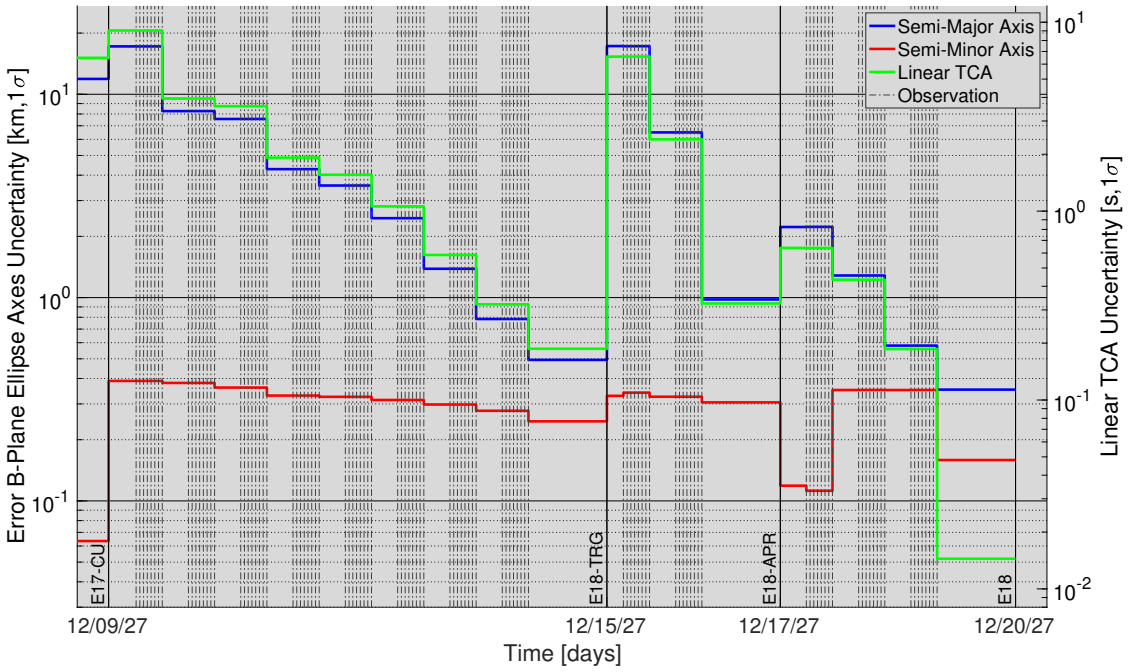

Fig. 7 Spacecraft state uncertainty mapped in B-plane coordinates for different times during the robust trajectory.

C. Epistemic Scenario

1. Epistemic Uncertainty Components

Epistemic uncertainty is considered in the initial dispersion and execution errors parameters. The initial dispersion considered in the aleatoric scenario is indeed the reconstructed uncertainty from simulated OD arcs post-flyby. Therefore, the values in Table 1 are estimated during the navigation analysis in the mission design phase, whereas the actual dispersion to consider during operations may vary from these values. This further uncertainty is modelled as epistemic, and the imprecise initial set is parameterised as

$$\begin{aligned} \mathcal{P}_{\mathbf{x}_0} = \{\, P_{\mathbf{X}_0} :\ & P_{\mathbf{x}_0} = \mathcal{N}\left(\mathbf{x}_0; \mu_{\mathbf{x}_0}, \widetilde{\sigma}^2_{\mathbf{x}_0}\right), \\ & \widetilde{\sigma}^2_{\mathbf{x}_0} = \text{blkdiag}(\, \lambda_{\mathbf{x}_{0-1}}\, \sigma^2_{\mathbf{x}_0}(1{:}3, 1{:}3),\ \lambda_{\mathbf{x}_{0-2}}\, \sigma^2_{\mathbf{x}_0}(4{:}6, 4{:}6)), \\ & \lambda_{\mathbf{x}_{0-1}} \in [0.5, 2.0],\ \lambda_{\mathbf{x}_{0-2}} \in [0.5, 2.0] \,\}\ , \end{aligned} \tag{40}$$

where $\sigma^2_{\mathbf{x}_0}(1{:}3, 1{:}3)$ and $\sigma^2_{\mathbf{x}_0}(4{:}6, 4{:}6)$ indicate respectively the position block and the velocity block of the covariance matrix $\sigma^2_{\mathbf{x}_0}$, the operator blkdiag indicates a block-diagonal matrix, $\lambda_{\mathbf{x}_{0-1}}$ and $\lambda_{\mathbf{x}_{0-2}}$ are two multipliers scaling the precise covariance matrix $\sigma^2_{\mathbf{x}_0}$ defined from the standard deviations in Table 1, independently for the position and velocity coordinates. Being the multipliers defined within $[0.5, 2.0]$, they encompass distributions with covariance from half up to double the magnitude of the pure aleatoric one.

For the execution errors, epistemic uncertainty is modelled by allowing interval-valued parameters in the Gates' model. Indeed, these parameters are estimated by testing the engine in nonoperational conditions, and then updated multiple times during the spacecraft operational life with possible substantial changes, e.g. during Cassini mission [36]. Specifically, the intervals for the model parameters considered in this analysis are reported in Table 5, which include the precise values previously employed.

2. Epistemic Belief Stochastic Formulation

The Europa's Clipper optimal control problem under epistemic uncertainty can be framed under the general formulation in Equation (10) as

Table 5 Gates' parameters of epistemic uncertainty model for execution errors considered in Europa's moon flyby stochastic optimisation.

Uncertainty	Component	Value	
Execution Error	Fixed Pointing	[1.67, 4.00]	[mm/s]
	Proportional Pointing	[3.33, 8.00]	[mrad]
	Fixed Magnitude	[2.33, 6.60]	[mm/s]
	Proportional Magnitude	[0.17, 0.40]%	[-]

$$\min_{\Delta\mathbf{v}_{k1}} \ \overline{\Delta V99} \tag{41a}$$

$$\text{s.t.} \quad \mathbf{X}_k = \mathcal{T}\left(\mathbf{X}_{k-1}, \Delta\mathbf{v}_{k-1}, \mathbf{D}_{k-1}, \mathcal{E}_k\right) \tag{41b}$$

$$\overline{Pr}_{TRG}\left(R_{E18} \leq R_{EUR}\right) < 0.1\% \tag{41c}$$

$$\mathbb{E}\left[\mathbf{B}_{E18}\right] = \overline{\mathbf{B}}_{E18} \tag{41d}$$

$$\mathbb{E}\left[\mathbf{R}_f\right] = \bar{\mathbf{r}}_f \tag{41e}$$

$$\mathbf{X}_0 \sim \mathcal{N}_{\mathbf{X}_0}\left(\boldsymbol{\mu}_{X_0}, \mathbf{P}_{X_0}\right), \tag{41f}$$

where $\overline{\Delta V99}$ and $\overline{Pr}_{TRG}$ are the upper bounds, resulting from the epistemic uncertainty, respectively for the $\Delta V99$ and PoI after targeting, computed as in Equation (9). This problem formulation corresponds to an epistemic worst-case scenario, where the optimisation is carried out conservatively to minimise the maximum propellant consumption while keeping the worst impact probability below a threshold as resulting from epistemic uncertainty.

3. Epistemic Robust Optimisation Results

The same initial solution as for the aleatoric case is employed for the stochastic optimisation of the epistemic scenario. The upper PoI bound is $2.29 \not< 0.1\%$, violating the chance constraint more severely than in the precise case as expected. The upper value for the $\Delta V99$ is significantly higher than the one in the aleatoric case, mainly due to larger execution errors considered (epistemic multiplier larger than one).

Table 6 Free variables, $\overline{\Delta V99}$ and upper Probability of Impact (PoI) for deterministic solution employed as first guess for stochastic epistemic optimisation.

Solution	$\Delta\mathbf{v}_{\text{CU-E17}}$ [m/s]	$\Delta\mathbf{v}_{\text{TRG-E18}}$ [m/s]	$\Delta\mathbf{v}_{\text{CU-E18}}$ [m/s]	Det ΔV [m/s]	$\overline{\Delta V99}$ [m/s]	$\overline{\Delta V99}$/Det ΔV [-]	$\overline{\text{PoI}}$ [-]
Deterministic	[0.0 , 0.0 , 0.0]	[−1.30, +2.86, +3.23]	[0.0 , 0.0 , 0.0]	4.51	8.65	1.92	2.29%

The corresponding B-plane uncertainty ellipses delivered from the maneuver instants along the trajectory are visualised in Figure 8. For each frame, multiple 3-σ ellipsoids are reported by sampling the epistemic uncertainty intervals with an Halton sequence and evaluating the stochastic transcription for each sample. By comparing with Figure 5, in every frame the possible delivered ellipses result changed in size and at times rotated due to the epistemic uncertainty considered. For the chance constraint on the PoI after targeting, the inner optimisation routine looks for the epistemic sample which yields to the ellipse with the largest intersection with the equivalent Europa surface in the top-right frame.

The feasible robust solution for Problem (41), found by the developed tool, is reported in Table 7. Again, the values of the expected value constraints are not reported as they are met up to the required threshold, that is the new trajectory respects the required flyby conditions and final position in expected value. The PoI after targeting constraint is satisfied by trading part of the targeting maneuver with the E17 and E18 clean-up maneuvers. The latter is now the largest maneuver employed to steer the spacecraft back to the desired final conditions. The value of the upper $\Delta V99$ is significantly higher than the precise one in Table 3 due to:

- the higher initial infeasibility (2.29% vs 0.75%) caused by the more severe epistemic uncertainty effects;
- the larger execution errors causing bigger deviations and therefore higher statistical $\delta\Delta V$s;

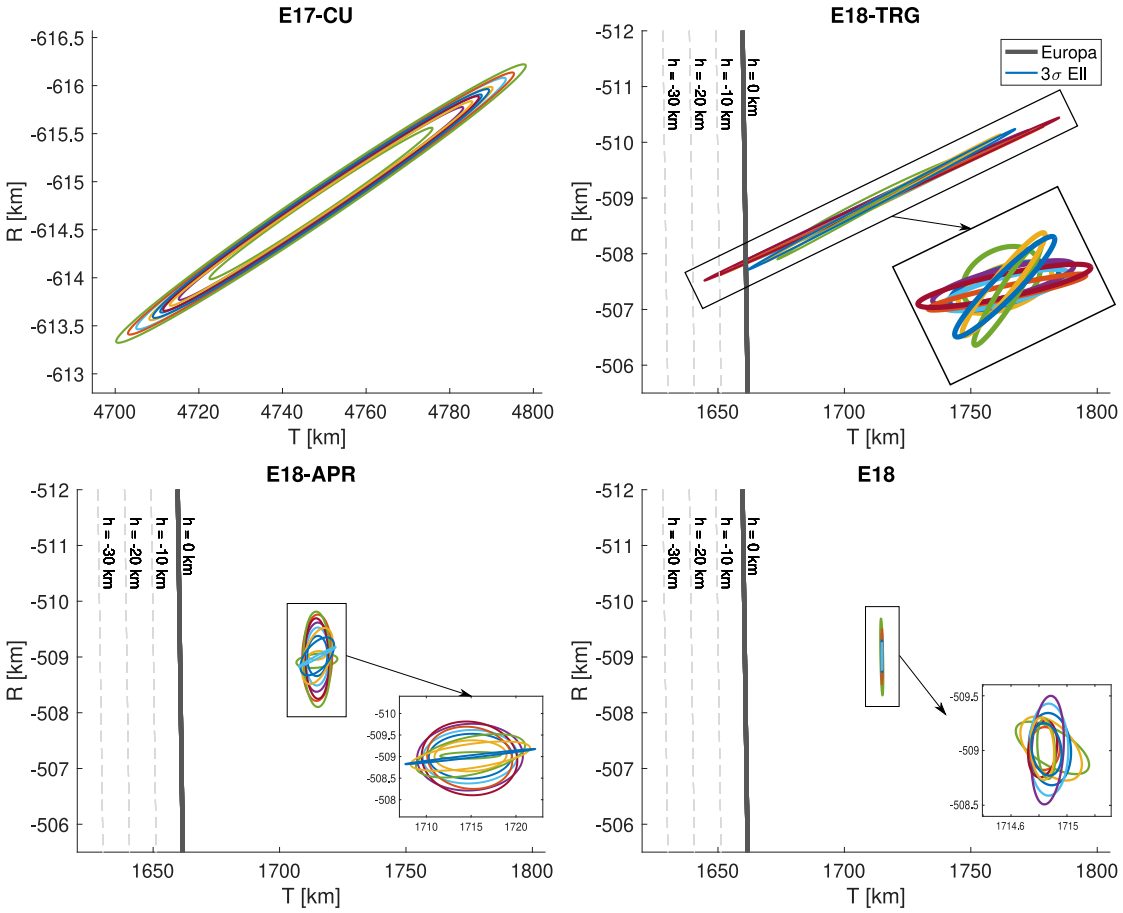

Fig. 8 Spacecraft delivered 3-σ confidence ellipses in B-plane parameters as mapped from the state uncertainty at different times along the deterministic trajectory without successive maneuvers and observations as resulting from both aleatoric and epistemic uncertainty.

Table 7 Free variables, $\overline{\Delta V99}$ and upper Probability of Impact (PoI) for robust epistemic solution optimised with the stochastic belief approach.

Solution	$\Delta\mathbf{v}_{\text{CU-E17}}$ [m/s]	$\Delta\mathbf{v}_{\text{TRG-E18}}$ [m/s]	$\Delta\mathbf{v}_{\text{CU-E18}}$ [m/s]	Det ΔV [m/s]	$\overline{\Delta V99}$ [m/s]	$\overline{\Delta V99}$/Det ΔV [-]	$\overline{\text{PoI}}$ [-]
Stochastic	[−0.35, +1.12, +0.16]	[−1.73, +1.57, +1.30]	[+1.43, −2.13, −3.24]	7.99	14.76	1.84	0.04%

- the upper bound $\overline{\Delta V99}$ is the epistemic worst case scenario, meaning that this budget is a conservative estimate given the ignorance coming from the epistemic structure of the problem.

A visualisation of the B-plane parameters 3-σ confidence ellipses for the robust solution is depicted in Figure 9, where again an Halton sequence has been used to sample the epistemic uncertainty.

By comparing it with Figure 8, the top-left plot displays an evident change in mapped B-plane parameters after E17-CU, as the larger clean-up maneuver steer the delivered uncertainty closer to the target flyby conditions. The top-right box, representing the mapped uncertainty after targeting, shows that there is no intersection between the largest 3-σ ellipse and the equivalent surface of Europa, confirming that the PoI constraint is met also in the epistemic case. Similarly to the precise case, the ellipses have smaller semi-major axes, larger semi-minor axes and are rotated counterclockwise to reduce the PoI while keeping the mean on the desired flyby conditions. The bottom-left plot reveals an increase in the delivered uncertainty after approach due to the larger statistical maneuvers. Finally, the bottom-right plot shows how the range and rangerate observations reduce the reconstructed uncertainty at flyby, mainly in the T-component, whereas the R-component results unobservable from the employed Earth-based measurements.

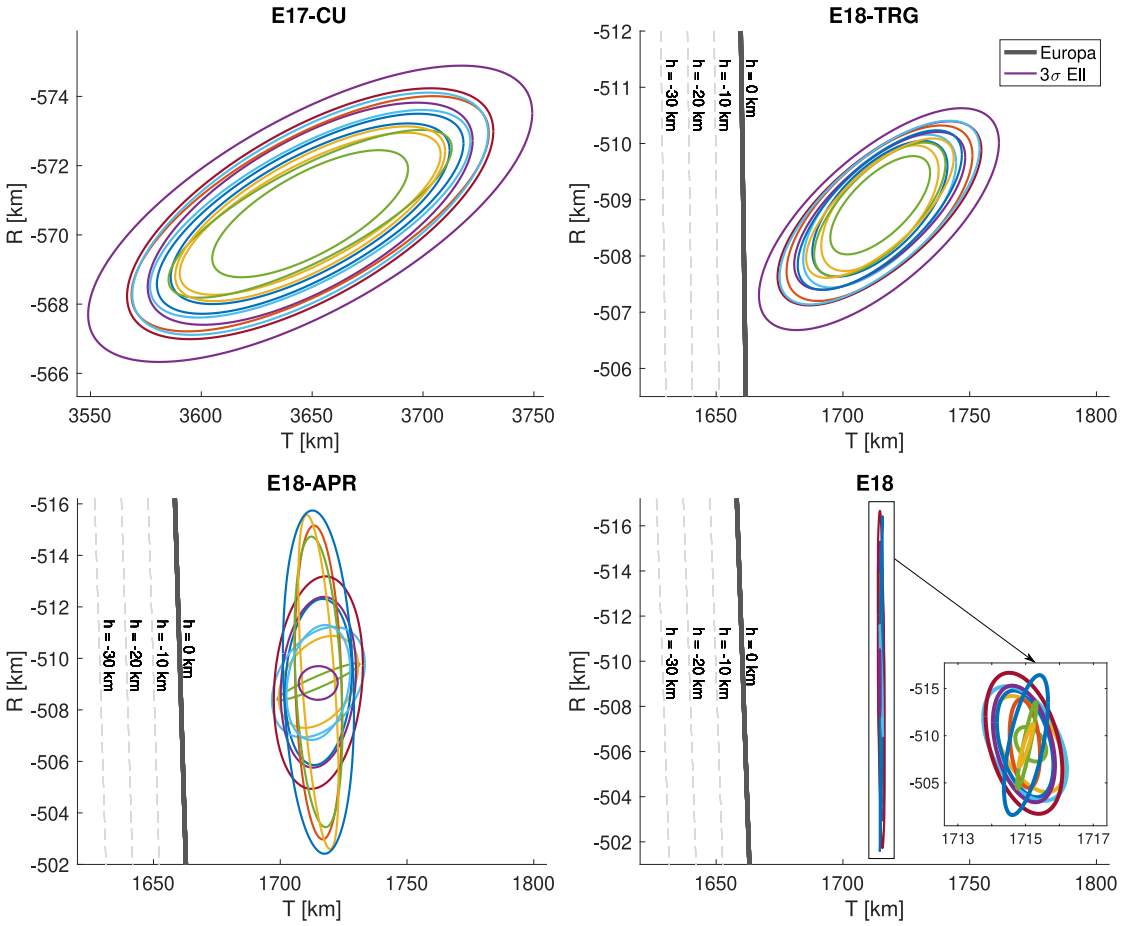

Fig. 9 Spacecraft delivered 3-σ confidence ellipses in B-plane parameters as mapped from the state uncertainty at different times along the robust trajectory without successive maneuvers and observations as resulting from both aleatoric and epistemic uncertainty.

V. Conclusions

This paper proposed novel developments in optimal control problems under uncertainty for the design of space trajectories with the goal of generating nominal trajectories which are both optimal and robust to the considered uncertainties.

The main contribution of this work is the generalisation of the OCPUU formulation and the corresponding stochastic transcription to the case of orbit determination arcs and statistical controllers.

The belief-based formulation presented can frame a large variety of problems in robust trajectory design, requiring no assumption on the uncertainty models to employ, which can be both aleatoric and epistemic. In addition, it encompasses also the case of joint thrust and sensor control optimisation. The introduced methodology enables the direct coupling of nominal trajectory optimisation with navigation analysis by working directly with a statistical objective index and stochastic constraints.

The developed transcription method, based on a stochastic shooting scheme, is composed of a propagation step, to map the uncertainty forward in time, and an update step, to incorporate the measurement information during orbit determination arcs. Hence, a new polynomial navigation analysis approach was developed to create a nonlinear, yet inexpensive, mapping of the dynamics to speed up the uncertainty propagation of the Monte Carlo samples over the observations.

In this work, the developed formulation and approach were successfully applied to the robust optimisation of a leg of Europa Clipper flyby tour subject to a chance constraint, namely the probability of impact with Europa, and constraints in expected value, namely flyby conditions and final position. Both aleatoric and epistemic uncertainties

were considered in the initial conditions, execution errors and observation noises. The belief stochastic optimisation was able to solve for the initial infeasibility in PoI of the deterministic optimum, and find a robust trajectory able to satisfy the statistical constraints while minimising the $\Delta V99$. As a verification, it was shown that the stochastic optimisation statistically outperformed the deterministic optimum $\Delta V99$ when no PoI is considered, that is when the deterministic trajectory is feasible.

Among possible future applications, the concurrent thrust and sensor control optimisation for joint trajectory and orbit determination planning could be addressed to find the optimal interactions between the control and estimation efforts. Furthermore, another suitable scenario where stochastic optimisation can result highly beneficial is the robust design of biasing maneuvers for planet flybys during interplanetary trajectories.

Acknowledgements

The authors would like to thank Eric Gustafson, Sonia Hernandez, Frank Laipert, Sumita Nandi, and Brian Young for sharing their expertise in navigation analysis and modelling for the addressed application, and for the insightful discussions during the approach development. Stefano Campagnola acknowledges the support from JPL's Research and Technology Development funds and from the Clipper project; part of this research was carried out at the Jet Propulsion Laboratory, California Institute of Technology, under a contract with the National Aeronautics and Space Administration. This work was partially funded by the European Commission's H2020 programme, through the H2020-MSCA-ITN-2016 UTOPIAE Marie Curie Innovative Training Network, grant agreement 722734.

References

[1] Rayman, M. D., and Williams, S. N., "Design of the first interplanetary solar electric propulsion mission," *Journal of Spacecraft and Rockets*, Vol. 3, 2002, pp. 589–595. doi:10.2514/2.3848.

[2] Laipert, F. E., and Longuski, J. M., "Automated Missed-Thrust Propellant Margin Analysis for Low-Thrust Trajectories," *Journal of Spacecraft and Rockets*, Vol. 52, 2015, pp. 1135–1143. doi:10.2514/1.A33264.

[3] Richards, A., and How, J., "Robust stable model predictive control with constraint tightening," *American Control Conference 2006 IEEE*, 2006. doi:10.1109/ACC.2006.1656440.

[4] Gustafson, E. D., "Stochastic Optimal Control of Spacecraft," Ph.D. thesis, The University of Michigan, 2010. doi:2027.42/77707.

[5] Olympio, J. T., and Yam, C. H., "Deterministic method for space trajectory design with mission margin constraints," *61st International Astronautical Congress*, Prague, Czech Republic, 2010.

[6] Olympio, J. T., "Designing Robust Low-Thrust Interplanetary Trajectories Subject to One Temporary Engine Failure," *20th AAS/AIAA Space Flight Meeting*, San Diego, CA, US, 2010.

[7] Ozaki, N., Campagnola, S., Funase, R., and Yam, C. H., "Stochastic Differential Dynamic Programming with Unscented Transform for Low-Thrust Trajectory Design," *Journal of Guidance, Control, and Dynamics*, Vol. 41, 2018, pp. 377–387. doi:10.2514/1.G002367.

[8] Vasile, M., "Robustness optimisation of aerocapture trajectory design using a hybrid co-evolutionary approach," *18th International Symposium on Space Flight Dynamics*, Munich, Germany, 2004.

[9] Zuiani, F., Vasile, M., and Gibbings, A., "Evidence-based robust design of deflection actions for near Earth objects," *Celestial Mechanics and Dynamical Astronomy*, Vol. 114, 2012, pp. 107–136. doi:10.1007/s10569-012-9423-1.

[10] Di Carlo, M., Vasile, M., Greco, C., and Epenoy, R., "Robust optimisation of low-thrust interplanetary transfers using evidence theory," *29th AAS/AIAA Space Flight Mechanics Meeting*, Ka'anapali, Hawaii, US, 2019. URL strathprints:67543.

[11] Greco, C., Di Carlo, M., Vasile, M., and Epenoy, R., "An intrusive polynomial algebra multiple shooting approach to the solution of optimal control problems," *Proceedings of the International Astronautical Congress, IAC , 2018*, Bremen, Germany, 2018. URL strathprints:65918.

[12] Stastny, N. B., and Geller, D. K., "Autonomous Optical Navigation at Jupiter: A Linear Covariance Analysis," *Journal of Spacecraft and Rockets*, Vol. 45, No. 2, 2008, pp. 290–298. doi:10.2514/1.28451.

[13] Geller, D. K., "Linear Covariance Techniques for Orbital Rendezvous Analysis and Autonomous Onboard Mission Planning," *Journal of Guidance, Control, and Dynamics*, Vol. 29, No. 6, 2006, pp. 1404–1414. doi:10.2514/1.19447.

[14] Kaelbling, L. P., Littman, M. L., and Cassandra, A. R., "Planning and acting in partially observable stochastic domains," *Artificial intelligence*, Vol. 101, No. 1-2, 1998, pp. 99–134. doi:10.1016/S0004-3702(98)00023-X.

[15] Greco, C., Gentile, L., Filippi, G., Minisci, E., Vasile, M., and Bartz-Beielstein, T., "Autonomous generation of observation schedules for tracking satellites with structured-chromosome GA optimisation," *2019 IEEE Congress on Evolutionary Computation (CEC)*, IEEE, 2019. doi:10.1109/CEC.2019.8790101.

[16] Gentile, L., Greco, C., Minisci, E., Bartz-Beielstein, T., and Vasile, M., "Structured-chromosome GA Optimisation for Satellite Tracking," *Proceedings of the Genetic and Evolutionary Computation Conference Companion*, ACM, New York, NY, USA, 2019. doi:10.1145/3319619.3326841.

[17] Gentile, L., Greco, C., Minisci, E., Bartz-Beielstein, T., and Vasile, M., "An optimization approach for designing optimal tracking campaigns for low-resources deep-space missions," *Proceedings of the International Astronautical Congress, IAC , 2019*, Washington, DC, US, 2019.

[18] Campagnola, S., Buffington, B. B., Lam, T., Petropoulos, A. E., and Pellegrini, E., "Tour Design Techniques for the Europa Clipper Mission," *Journal of Guidance, Control, and Dynamics*, 2019, pp. 1–12. doi:10.2514/1.G004309.

[19] Bagchi, A., *Optimal control of stochastic systems*, Prentice Hall International (UK) Limited, 1993.

[20] Krishnamurthy, V., *Partially observed Markov decision processes*, Cambridge University Press, 2016.

[21] Sarkka, S., *Bayesian Filtering and Smoothing*, 1st ed., Cambridge University Press, New York, 2013.

[22] Jeffrey, R. C., *The Logic of Decision*, 2nd ed., University of Chicago Press, 1983.

[23] Xiu, D., and Karniadakis, G. E., "The Wiener–Askey polynomial chaos for stochastic differential equations," *SIAM journal on scientific computing*, Vol. 24, 2002, pp. 619–644. doi:10.1137/S1064827501387826.

[24] Vasile, M., Ortega Absil, C., and Riccardi, A., "Set propagation in dynamical systems with generalised polynomial algebra and its computational complexity," *Communications in Nonlinear Science and Numerical Simulation*, Vol. 75, 2019, pp. 22–49. doi:10.1016/j.cnsns.2019.03.019.

[25] Bäck, J., Nobile, F., Tamellini, L., and Tempone, R., "Stochastic spectral Galerkin and collocation methods for PDEs with random coefficients: a numerical comparison," *Spectral and High Order Methods for Partial Differential Equations*, Lecture Notes in Computational Science and Engineering, Vol. 76, edited by J. Hesthaven and E. Ronquist, Springer, 2011, pp. 43–62.

[26] Ortega, C. A., Serra, R., Riccardi, A., and Vasile, M., "De-orbiting and re-entry analysis with generalised intrusive polynomial expansions," *67th International Astronautical Congress*, 2016. URL strathprints:60596.

[27] Riccardi, A., Tardioli, C., and Vasile, M., "An intrusive approach to uncertainty propagation in orbital mechanics based on Tchebycheff polynomial algebra," *Advances in Astronautical Sciences*, 2015, pp. 707–722. URL strathprints:60560.

[28] Ito, K., and Xiong, K., "Gaussian filters for nonlinear filtering problems," *IEEE Transactions on Automatic Control*, Vol. 45, No. 5, 2000, pp. 910–927. doi:10.1109/9.855552.

[29] Greco, C., Gentile, L., Vasile, M., Minisci, E., and Bartz-Beielstein, T., "Robust particle filter for space objects tracking under severe uncertainty," *2019 AAS/AIAA Astrodynamics Specialist Conference*, Portland, ME, US, 2019. URL strathprints:70566.

[30] Lynam, A. E., and Longuski, J. M., "Preliminary analysis for the navigation of multiple-satellite-aided capture sequences at Jupiter," *Acta Astronautica*, Vol. 79, 2012, pp. 33–43. doi:10.1016/j.actaastro.2012.04.012.

[31] Campagnola, S., Ozaki, N., Sugimoto, Y., Yam, C. H., Chen, H., Kawabata, Y., Ogura, S., Sarli, B., Kawakatsu, Y., Funase, R., and Nakasuka, S., "Low-thrust trajectory design and operations of PROCYON, the first deep-space micro-spacecraft," *24th International Symposium on Space Flight Dynamics*, Munich, Germany, 2015.

[32] Gates, C. R., "A simplified model of midcourse maneuver execution errors," Tech. rep., Jet Propulsion Laboratory, California Institute of Technology, 1963.

[33] Boone, D. R., Nandi, S., Kangas, J., and Young, B., "Orbit Determination Sensitivity Analysis for the Europa Multiple Flyby Mission Concept," *AIAA/AAS Astrodynamics Specialist Conference*, 2016. doi:10.2514/6.2016-5429.

[34] Nandi, S., Kangas, J., Valerino, P. N., Buffington, B., Ionasescu, R., and Boone, D., "Initial navigation analysis for the Europa multiple flyby mission concept," *26th AAS/AIAA Space Flight Mechanics Meeting*, 2016.

[35] Valerino, P. N., Buffington, B., Criddle, K., Hahn, Y., Ionasescu, R., Kangas, J. A., Martin-Mur, T., Roncoli, R. B., and Sims, J. A., "Preliminary Maneuver Analysis for the Europa Clipper Multiple-Flyby Mission," *AIAA/AAS Astrodynamics Specialist Conference*, 2014. doi:10.2514/6.2014-4461.

[36] Wagner, S. V., "Cassini Maneuver performance assessment and execution-error modeling through 2015," *26th AAS/AIAA Space Flight Mechanics Meeting*, Napa, CA, US, 2016.